Modelling SO_2 conversion into sulphates in the mid-troposphere with a 3D chemistry-transport model: the case of Mount Etna's eruption on April 12, 2012.

Mathieu Lachatre[1,5], Sylvain Mailler[1,2], Laurent Menut[1], Arineh Cholakian[1], Pasquale Sellitto[3], Guillaume Siour[3], Henda Guermazi[3], Giuseppe Salerno[4], and Salvatore Giammanco[4]

[1]LMD/IPSL, École Polytechnique, Institut Polytechnique de Paris, ENS, PSL Université, Sorbonne Université, CNRS, Palaiseau, France.
[2]École des Ponts, Université Paris-Est, 77455 Champs-sur-Marne, France.
[3]Univ Paris Est Creteil and Université de Paris, CNRS, LISA, F-94010 Créteil, France
[4]Istituto Nazionale di Geofisica e Vulcanologia, Osservatorio Etneo, Catania, Italy.
[5]Presently at ARIA is now SUEZ, 8-10 rue de la Ferme 92100 Boulogne-Billancourt France

Correspondence: Mathieu Lachatre (mathieu.lachatre@suez.com)

Abstract. Volcanic activity is an important source of atmospheric sulphur dioxide (SO_2), which, after conversion into sulphuric acid, induces impacts on, among others, rain acidity, human health, meteorology and the radiative balance of the atmosphere. This work focuses on the conversion of SO_2 into sulphates ($SO_{4(p)}^{2-}$, $S(+VI)$) in the mid-tropospheric volcanic plume emitted by the explosive eruption of Mount Etna (Italy) on Apr. 12, 2012, using the CHIMERE chemistry-transport model. Since volcanic plume location and composition depend on several often poorly constrained parameters, using a chemistry-transport model allows us to study the sensitivity of SO_2 oxidation to multiple aspects such as volcanic water emissions, transition metal emissions, plume diffusion and plume altitude. Our results show that in the mid-troposphere, two pathways contribute to sulphate production, the oxidation of SO_2 by OH in the gaseous phase (70 %), and the aqueous oxidation by O_2 catalyzed by Mn^{2+} and Fe^{3+} ions (25 %). The oxidation in aqueous phase is the faster process, but in the mid-troposphere, liquid water is scarce, therefore the relative share of gaseous oxidation can be important. After one day in the mid-troposphere, about 0.5 % of the volcanic SO_2 was converted to sulphates through the gaseous process. Because of the nonlinear dependency of the kinetics in the aqueous phase to the amount of volcanic water emitted and on the availability of transition metals in the aqueous phase, several experiments have been designed to determine the prominence of different parameters. Our simulations show that during the short time that liquid water remains in the plume, around 0.4 % of sulphates manage to quickly enter the liquid phase. Sensitivity tests regarding the advection scheme have shown that this scheme must be chosen wisely, as dispersion will impact both oxidation pathways explained above.

1 Introduction

Sulphate aerosols resulting from the conversion of volcanic sulphur dioxide (SO_2) have substantial effects on air quality, meteorology, rain acidity and the radiative balance of Earth atmosphere at local-to-global spatial scales, depending on the

specific volcanic activity (e.g. Langmann (2014); Sellitto et al. (2017); Pattantyus et al. (2018); Sellitto et al. (2191)). SO_2 is emitted from both anthropogenic and natural sources, volcanic emissions being the major contributors to the natural emissions. Volcanic emissions can be classified as coming from two broad classes of volcanic activity: passive degassing and explosive events. Passive degassing occurs permanently at many volcanoes. For example, Etna emits an estimated $530\,kt\,yr^{-1}$ of SO_2 annually, making it the eighth contributor to SO_2 emissions from passive degassing; the strongest contributor worldwide being Mount Kilauea (in Hawai, USA), which emits an estimated $2740\,kt\,yr^{-1}$ annually (Itahashi et al. (2021)). Explosive eruptions emit massive quantities of SO_2 into the atmosphere in a short period of time. Unlike passive degassing, which generates emissions close to the surface, explosive eruptions may emit SO_2 high above the volcanic vent, with the possibility of getting up to the stratosphere for massive eruptions such as El Chichón in 1982 (Pollack et al., 1983) or Mount Pinatubo (Philippines) in 1992, or even the more moderate recent activity of volcanoes such as Raikoke (e.g. Kloss et al. (2021)).

While contributing to the air quality on a local-to-regional scale, the sulphate aerosols produced as a result of explosive volcanic activities represent an important natural radiative forcing as well and are therefore significant for climate studies. Pattantyus et al. (2018) give an extensive review of the oxidation processes of SO_2 in the Marine boundary layer for the case of Mount Kilaueaa, and list two main oxidation paths for this species, oxidation by hydroxyl radical (OH) in gas phase, and oxidation in liquid phase (including oxidation by H_2O_2, O_3 and catalytic oxidation via O_2). However, its fate in volcanic plumes in the free troposphere still remains poorly understood, in part due to the difficulty of measuring these events. Multiple efforts have been carried out to understand and model sulphates formation within volcanic plumes, mostly at first phases of eruption events (Hoshyaripour et al., 2014, 2015; Roberts et al., 2019). Heard et al. (2012) have modelled the plumes from Kasatochi in 2008 , Mt. Sarychev in 2009, and Eyjafjallajökull in 2010 with the NAME dispersion model, with encouraging results in reproducing the observed plumes of SO_2 and sulphates. Specific modelling work has been carried out using a 0D model (Galeazzo et al., 2018), and brought interesting insights into main oxidation pathways of SO_2: these authors highlight on the potential importance of the catalytic oxidation of SO_2 by O_2 with transition metals as catalysts. Pianezze et al. (2019) and Sahyoun et al. (2019) have explored the role of ~~volcanic aerosols as Cloud Condensation Nuclei (CCN) and the evolution of~~ secondary sulphate aerosols in the volcanic plumes from Etna and Stromboli, showing that these secondary aerosols are initially nucleated with very small diameters, but that their size distribution ~~. In the free troposphere, volcanic particle size distribution~~ is evolving to a coarser distribution as time goes by ~~, and~~ so that these sulphate particles can serve as CCN far from the vent~~(Sahyoun et al., 2019; Pianezze et al., 2019)~~.

Regarding mid-tropospheric eruptions, the issue of aqueous chemistry, with the potential contribution of volcanic water emissions to the formation of an aqueous phase needs to be considered since there is the possibility that these emissions have an impact on sulphate formation for this portion of the atmosphere. In the case of boundary layer eruptions and passive degassing, the quantity of water vapour emitted by the volcano is typically much smaller than the background water vapour at that level, while for stratospheric eruptions temperatures are too cold to allow the presence of liquid water. In particular, the question of sensitivity of sulphate formation to the volcanic emissions of water vapour is unanswered as of yet. In addition, the 0D study of Galeazzo et al. (2018) argues that aqueous oxidation of SO_2 catalyzed by transition metals may be a substantial, or even dominant, oxidation pathway, and that explosive eruptions themselves emit water vapour (possibly contributing to the

formation of an atmospheric liquid phase) and transition metals. Another effect, not taken into account in the present study, is the potential depletion of OH radicals due to its consumption by atmospheric halogen. Jourdain et al. (2016) conducted a modelling study on the volcanic plumes of the Ambrym volcano (Vanuatu). They conclude that when taking into account halogen emissions, the lifetime of SO_2 relative to oxidation by OH increases by 36% compared to the same simulation without halogen emissions; the authors attribute this change to OH depletion.

Various pathways can lead to SO_2 [S(+IV)] oxidation to SO_4^{2-} [S(+VI)]. In the gaseous phase, SO_2 can react with the OH photochemically produced from ozone and water vapour:

$$O_{3(g)} \;+\; h\nu \;\longrightarrow\; O_2 + O(^1D) \tag{R1}$$

$$O(^1D) \;+\; H_2O \;\longrightarrow\; 2OH \tag{R2}$$

Gas-phase conversion of SO_2 by OH follows reactions R3-R5 (Seinfeld and Pandis, 2006):

$$SO_{2(g)} + OH + M \;\longrightarrow\; HOSO_{2(g)} + M \tag{R3}$$

$$HOSO_{2(g)} \;+\; O_2 \;\longrightarrow\; HO_2 + SO_{3(g)} \tag{R4}$$

$$SO_{3(g)} \;+\; H_2O \;\longrightarrow\; H_2SO_{4(g)} + M. \tag{R5}$$

Reaction R3, the limiting step in this mechanism, is relatively slow (the decay rate of SO_2 through this mechanism is estimated at $2.9 \pm 2.1 \,\%\,h^{-1}$ during daytime for the remote marine conditions around Mt. Kilauea), therefore in presence of an aqueous phase liquid-phase conversion tends to dominate gas-phase conversion.

Since SO_2 is a soluble gas, aqueous-phase oxidation is also a possibility; the balance between liquid-phase and gas-phase concentrations being governed by the Henry's law:

$$[SO_2]_{aq} = H_{SO_2} p_{SO_2}, \tag{1}$$

where $[SO_2]_{aq}$ is the concentration of dissolved SO_2 in the aqueous phase, p_{SO_2} the partial pressure of SO_2 in gas phase and H_{SO_2} is Henry's law constant for SO_2, for which the expression and numerical parameters can be found in e.g., Sander (2015):

$$H_{SO_2}(T) = H_{SO_2}^0 \exp\left[B\left(\frac{1}{T} - \frac{1}{T^0} \right) \right], \text{with} \tag{2}$$

$$H_{SO_2}^0 = 1.3 \times 10^{-2}\,mol\,m^{-3}\,Pa^{-1},\ B = 2900\,K \text{ and } T^0 = 298.15\,K \tag{3}$$

Aqueous SO_2 solution behaves like a weak acid, known as "sulfurous acid":

$$SO_{2(aq)} + H_2O \rightleftharpoons H^+ + HSO_3^-, \tag{R6}$$

with

$$\frac{[\mathrm{H}^+][\mathrm{HSO}_3^-]}{[\mathrm{SO}_{2(\mathrm{aq})}]} = \mathrm{K}_a^{\mathrm{H_2SO_3}}, \tag{4}$$

with a weak acidity constant of $\mathrm{pK}_a^{\mathrm{H_2SO_3}} = 1.81$.

For the sake of completeness, it should also be mentioned that sulfurous acid can have a second acidic dissociation:

$$\mathrm{HSO}_3^- \rightleftharpoons \mathrm{H}^+ + \mathrm{SO}_3^{2-} \tag{R7}$$

with $\mathrm{pK}_a^{\mathrm{HSO_3^-}} = 7.21$, but for pH values below 6 usually occurring in the atmosphere, this second dissociation hardly has an impact. In typical atmospheric conditions (including those found in volcanic plumes) with a pH between 2 and 7, aqueous S(+IV) is seen mainly in the form of HSO_3^- (Seinfeld and Pandis, 2006). One pathway for oxidation of S(+IV) to S(+VI) in aqueous phase is reaction of HSO_3^- with hydrogen peroxide $\mathrm{H}_2\mathrm{O}_2$ (e.g. Shostak et al. (2019)):

$$\mathrm{HSO}_{3(\mathrm{aq})}^- + \mathrm{H}_2\mathrm{O}_{2(\mathrm{aq})} \quad \rightarrow \quad \mathrm{SO}_2\mathrm{OOH}_{(\mathrm{aq})}^- + \mathrm{H}_2\mathrm{O} \tag{R8}$$

$$\mathrm{SO}_2\mathrm{OOH}_{(\mathrm{aq})}^- + \quad \mathrm{H}^+ \quad \rightarrow \quad \mathrm{H}_2\mathrm{SO}_{4(\mathrm{aq})} \tag{R9}$$
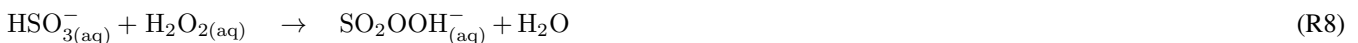
However, in situations resembling volcanic plumes where SO_2 is abundant, the availability of $\mathrm{H}_2\mathrm{O}_2$ is a limiting factor for R8 and hence other reaction pathways become dominant (Pattantyus et al., 2018). In such cases, oxidation of $\mathrm{HSO}_{3(\mathrm{aq})}^-$ by O_3 can become an important pathway (reaction R10; Lagrange et al., 1994; Seinfeld and Pandis, 2006; Pattantyus et al., 2018):

$$\mathrm{HSO}_{3(\mathrm{aq})}^- + \mathrm{O}_{3(\mathrm{aq})} \quad \rightarrow \quad \mathrm{H}^+ + \mathrm{SO}_{4(\mathrm{aq})}^{2-} + \mathrm{O}_{2(\mathrm{aq})} \tag{R10}$$

Finally, oxidation of $\mathrm{HSO}_{3(\mathrm{aq})}^-$ by O_2 with Fe^{3+} and Mn^{2+} as catalysts is another process that can be relevant in our case: (reaction R11; Connick and Zhang, 1996).

$$\mathrm{HSO}_{3(\mathrm{aq})}^- + \frac{1}{2}\mathrm{O}_{2(\mathrm{aq})} \xrightarrow{Fe^{3+},\,Mn^{2+}} \mathrm{SO}_{4(\mathrm{aq})}^{2-} + \mathrm{H}^+ \tag{R11}$$

The aim of this work is to estimate the sensitivity of SO_2 conversion through these pathways in a volcanic plume to several parameters that remain poorly constrained.

From a modelling point of view, Lachatre et al. (2020b) has shown that using the Després and Lagoutière (1999) antidiffusive advection scheme in the vertical direction rather than the classical order-2 Van Leer (1977) scheme substantially reduces plume diffusion, reducing plume volume and increasing its concentration. With this antidiffusive scheme, the plume volume is reduced by a factor ranging from 1.5 to 6 relative to the Van Leer (1977) scheme (depending on model configuration, see Lachatre et al. (2020b) for details). Due to the many nonlinearities in the above-described physico-chemical mechanisms governing SO_2 oxidation, the effect of such a change in numerical diffusion on the way the model represents sulphate formation is not straightforward: too much numerical diffusion in a model may enhance certain oxidation processes (such as oxidation by the background tropospheric species such as OH or $\mathrm{H}_2\mathrm{O}_2$, which can be limited by the availability of these oxidants when the plume stays concentrated), and reduce others (such as aqueous-phase oxidation of SO_2) which can be favored by the simultaneous presence of large concentrations of volcanic water and volcanic SO_2. To examine these effects, it is also relevant to quantify the impact of these advection choices on the various oxidation paths of SO_2.

In Section 2, we present the data used in the current study and the modelling choices that have been made. Section 3 presents the simulation outputs and their interpretation in terms of comparison to observations and in terms of sensitivity to multiple parameters. Finally, Section 4 draws conclusions and examines new perspectives that are not covered by the present study.

2 Material and methods

2.1 IASI instrument

The Infrared Atmospheric Sounding Interferometer (Clarisse et al., 2014, IASI) instrument onboard of Metop-A-C satellite series, the instrument is orbiting 817 km above the surface and provides a daily coverage of the earth with a pixel resolution of 12 km of diameter. IASI retrievals are widely used to observe and study the SO_2 in the Earth's atmosphere Clarisse et al. (2012), including in volcanic plumes Carboni et al. (2012, 2016). This instrument has also been recently used to measure the Aerosol optical depth (AOD) of tropospheric volcanic sulphate particles (Guermazi et al., 2021).

2.2 CHIMERE model

The modelling work has been performed using v2020r1 version of the CHIMERE CTM (chemistry-transport model) (derived from v2020r1; Mailler et al., 2017; Menut et al., 2021) including new developments for vertical transport presented in Lachatre et al. (2020b); Mailler et al. (2020). The CHIMERE simulation domain covers the Central-Eastern mediterranean basin and contains 874×624 cells at $2.25 \times 2.25 \, \text{km}^2$ horizontal resolution. The geometry of the domain, which has a Lambert-conformal projection, was chosen to contain volcanic plume transport for a day, with a sufficiently fine resolution to resolve the volcanic plume during the first hours of its atmospheric advection (domain is displayed on Figure A2, in the appendix). At model resolution, the cell containing the vent has an average altitude of 2900 m.a.s.l.. The vertical distribution of the domain contains 40 layers, with the top of the domain being at 190 hPa. Horizontal advection in the CHIMERE model has been represented using the classical Van Leer (1977) second-order slope-limited transport scheme.

Anthropogenic emissions are generated using the HTAP 2010 inventory (Janssens-Maenhout et al., 2015), boundary conditions for dust are calculated from GOCART global model (Ginoux et al., 2001) and from the global model LMDZ-INCA (Hauglustaine et al., 2004) for other species. The CHIMERE model has been forced using WRFv.3.7.1 (Weather Research and Forecasting Skamarock et al., 2008), with an update of the forcing meteorological variables every 20 minutes using the WRF-CHIMERE online simulation framework (Briant et al., 2017; Menut et al., 2021). The WRF model has been run with 44 vertical levels starting from surface to 50 hPa with the same horizontal grid as the one used for CHIMERE. Large-scale meteorological fields used to force the WRF model at domain boundaries as well as for spectral nudging inside the simulation domain have been taken from the NCEP GFS dataset at 0.25° resolution (NCEP, 2015). The chemical modelling is as described in Mailler et al. (2017) (and references therein), including the reduced MELCHIOR2 chemical mechanism for inorganic chemistry, SO_x chemistry , OH chemistry and more (Derognat et al., 2003; Menut et al., 2013). Gaseous oxidation pathways and aqueous oxidation through O_3 and H_2O_2 are included in this mechanism, and no modifications were made

on this aspect of the chemistry mechanism. For the present study, retroaction from atmospheric composition onto the WRF simulation is not activated, meaning that all the chemistry-transport simulations are forced by the exact same meteorological fields, which permits to isolate the physico-chemical effects of the volcanic eruption from the complex feedback it may have on the meteorological fields.

For radiative porcesses, calculations are done online using the Fast-JX module (version 7.0b, see Bian and Prather, 2002). As described in Mailler et al. (2016), the CHIMERE model includes the feedback of aerosol layers on photolysis rates. The calculation of the Aerosol optical depths is also done by the Fast-JX module, using Mie calculations assuming spherical shape for all particles and external mixing.

Oxidation of SO_2 by $O_{2(aq)}$ catalyzed by Fe and Mn is also available in the model; the evaluation of $[Fe^{3+}]$ and $[Mn^{2+}]$ have been adapted for the present study as discussed in Section 2.5.

2.3 Modelling Volcanic eruption emissions

The time and altitude profiles for the injection of SO_2 into the atmosphere (Table 1) were obtained using SO_2 emission flux rate measurement data from the ground-based DOAS FLAME (Differential Optical Absorption Spectroscopy FLux Automatic MEasurements) scanning network (e.g. Salerno et al., 2018). This method measures SO_2 fluxes during passive degassing, effusive and explosive eruptive activity using plume height inverted via an empirical relationship between plume height and wind speed (Salerno et al., 2009). In explosive paroxysmal events, such as in our case study, the plume is ejected to higher altitudes and the linear height-wind relationship explained above cannot be utilized; therefore mass flux is retrieved in post-processing using the plume height estimated by visual camera and/or satellite observations.

On April 12, 2012, between 06 UTC and 16 UTC, a total SO_2 emission of 8.6 kt was reported by this method. Emissions are localized around 8 km.a..s.l.. Volcanic SO_2 emissions are injected in the CTM with a skewed Gaussian profile (Eckhardt et al., 2008; Mastin et al., 2009). The width of the Gaussian is defined by Full Width at Half Maximum (FWHM, equation 5) and it equals to 5 % of the center of injection's altitude ($\bar{x}$). The Gaussian profile is constructed with 13 altitude ranges, with widths corresponding to 1 % of the center of injection altitude.

$$\sigma = \frac{FWHM}{2.355} = \frac{\bar{x} \times 0.05}{2.355} \tag{5}$$

Volcanic emissions from explosive activities are more likely to be described with a skewed Gaussian profile (equation 6). In our case, we have selected a coefficient of skewness of $\alpha = 0.5\,\mathrm{m}$. Center of the injection is localized at 8 000 m.a.s.l. ($\bar{x}$ value used to calculate $FWHM$); thus, $FWHM$ equals to 400 m and σ^2 to 170 m using equation 6. The vertical distribution is then constructed within 13 altitude ranges, with a width equal to 80 m (1 % of $\bar{x}$). The center of the injection is the center of the 7th range. The entry for eruptive material in CHIMERE, before it is adapted to CHIMERE vertical grid, is displayed on Figure A1. Water, Fe and Mn are emitted with the identical vertical distribution.

$$f(x) = \frac{\sqrt{2}}{\sqrt{\pi}(\sigma + \alpha)} \times \left[e^{\frac{-(x-\bar{x})^2}{2\sigma^2}} \times \mathbf{1}_{]-\infty;\bar{x}]}(x) + e^{\frac{-(x-\bar{x})^2}{2\alpha^2}} \times \mathbf{1}_{]\bar{x};\infty[}(x) \right] \tag{6}$$

Table 1. SO_2 hourly flux $(kg.s^{-1})$ estimates used as input for the CHIMERE model.

date	time	SO_2 flux $(kg.s^{-1})$	SO_2 mass (t)	Fe mass (t)	Mn mass (t)
12/04/2012	06 UTC	249.9	899.6	0.78	0.077
12/04/2012	07 UTC	400.9	1443.4	1.26	0.124
12/04/2012	08 UTC	186.7	672.4	0.59	0.058
12/04/2012	09 UTC	234.7	844.9	0.74	0.072
12/04/2012	10 UTC	276.5	995.3	0.87	0.085
12/04/2012	11 UTC	173.0	623.0	0.54	0.054
12/04/2012	12 UTC	202.9	730.5	0.64	0.062
12/04/2012	13 UTC	321.7	1158.2	1.01	0.099
12/04/2012	14 UTC	199.1	716.9	0.63	0.061
12/04/2012	15 UTC	144.4	519.9	0.45	0.044

2.4 Volcanic water emissions

Volcanic eruptions inject significant amounts of water in the atmosphere, particularly when considering the ambient humidity in the mid and upper troposphere. In the experiments containing volcanic water emissions, H_2O is emitted similarly to SO_2 emissions, with identical time and vertical profiles as described in Section 2.3; To estimate the specific amount of the emitted H_2O, a molecular ratio between SO_2 and H_2O has been implemented. For passive degassing, Shinohara et al. (2008) estimate the molecular H_2O/SO_2 ratio be around 45 when considering 27 events, and 26 when considering 13 events with the highest quality of data sampling, with a large variability. Nonetheless, explosive episodes eject water significantly larger amount, with H_2O/SO_2 molecular ratios likely reaching values of several hundreds, and the H_2O/SO_2 ratios associated to these events still carry large uncertainties. To assess the sensitivity of our results to this ratio, we have tested several hypotheses for the H_2O/SO_2 ratio. As observational information is scarcely available for volcanic water emissions during explosive events, a central hypothesis of 300 molecules of H_2O per molecules of SO_2 has been retained, corresponding to $725.6\,kt_{H_2O}$.

Addition of volcanic water in the mid-troposphere can imply supersaturation. Consequently, in the model, water is added as water vapour until the partial pressure of water vapour reaches $105\,\%$ of the saturation vapour pressure $P_{H_2O}^{sat}$. Remaining water emitted from the eruptive activity is added as liquid water or ice, depending on ambient temperature. Several studies have focused on the phase state of water in the upper troposphere (Textor et al., 2003; Hu et al., 2010; Kärcher and Seifert, 2016) and it is generally agreed that liquid water is virtually inexistent below the temperature of $\simeq 235\,K$. Based on CALIOP measurements, Komurcu et al. (2014) has evaluated the supercooled liquid water fraction in clouds. Based on their Fig. 7,

Eq. 7 gives a parabolic dependance of the supercooled liquid water fraction $H_2O_{(s)}$ on temperature, to be used between 235 and 273K (function is plot on Figure A3, in the appendix):

$$\%H_2O_{(s)} = -22.49 + 0.2092 \times T - 0.0004649 \times T^2 \tag{7}$$

2.5 Transition Metal Ions (TMI) dissolution into droplets and $[Fe^{3+}]_{(aq)}$ and $[Mn^{2+}]_{(aq)}$ threshold

In addition to SO_2 and water, volcanic eruptions inject significant amounts of transition metals into the atmosphere, such as Fe and Mn (Calabrese et al., 2011). These trace elements can be contained in the emitted volcanic ash, which is more relevant during volcanic eruptive activity and must be considered in our simulations because of their catalytic role in the aqueous oxidation of SO_2 by O_2 (reaction R11). In our simulations, the amount of transition metals emitted by the volcano are defined relative to SO_2 emissions, with a molecular ratio of 1/1000 (i.e. 7.5 t) and 1/10000 (i.e. 0.73 t) respectively for Fe and Mn. The SO_2 oxidation to sulphate is catalyzed by $Mn^{2+}_{(aq)}$ and $Fe^{3+}_{(aq)}$ ions. The fraction of Fe^{3+} in cloud droplets and available to the catalytic reaction is a complex matter which depends of several factors ($H_2S_{(g)}$ / $H_{2(g)}$ Hoshyaripour et al. 2014; Halogen content $[Cl^-]$ Maters et al. 2017; ashes' surface and bulk compositions). In an ideal situation, up to a third of the total Fe on the ash surface can dissolve into the liquid phase coating volcanic particles, mostly in Fe(II) oxidation state (Galeazzo et al., 2018; Hoshyaripour et al., 2015). In our experiments, we consider 5 % of the total Iron and Manganese in the plume to be dissolved in the liquid phase (if clouds are produced) and therefore are available as catalysts for Reaction R11. In the case of liquid water in the plume, the Iron concentration in droplets ($mol.L^{-1}$) is calculated following the equation :

$$[Fe^{3+}_{(aq)}]_{i,j,l,t} = \frac{[Fe]_{i,j,l,t} \times 0.05 \times (1 - icefrac_{i,j,l,t}) \times V_{i,j,l,t}}{M_{Fe} \times VH_2O_{i,j,l,t}} \tag{8}$$

where i, j, l, t are the cell coordinates and time steps, M_{Fe} the molar mass of Iron ($\mu g.mol^{-1}$), VH_2O the volume of Super Cooled Liquid Water (SCLW; L), V the volume of the cell (m^3), $[Fe_{(g)}]$ the concentration of Iron in the atmosphere ($\mu g.m^{-3}$) and $icefrac$ is the fraction of ice cloud compared to liquid water (c.f. No Section 2.4).

The second parameter that needs to be fixed is the upper limit for $[Fe(III)]$. Seinfeld and Pandis (2006) indicate a range of Iron concentrations from 0.1 to 100 $\mu mol.L^{-1}$ in clouds, a large range compared to more recent studies, estimating $[Fe(III)]$ from 0.1 to 2 $\mu mol.L^{-1}$ (Maters et al., 2016, 2017). Fe^{3+} is more likely to be dissolved in an acidic cloud droplet (pH below 2; Ayris and Delmelle, 2012), this particular condition can lead to $[Fe(III)]$ going up to 10 μM (Ayris and Delmelle, 2012; Desboeufs et al., 2001). In our experiments, volcanic cloud droplets are particularly acidic, with a pH ranging from 1.5 to 3.5. In consequence, thresholds of 10 $\mu mol.L^{-1}$ for $[Fe(III)]$ and 1 $\mu mol.L^{-1}$ for $[Mn(II)]$ were chosen.

2.6 ~~Simulations conducted and their purpose~~Description of numerical simulations

Simulations have been organized into groups, to explore various parameters of interest. First, the simulations focused on the significance of gas phase conversion, aqueous phase conversion and transition metals as catalysts are gathered (Table 2). Then,

we focused on the impact of volcanic water emitted during volcanic activity (Table 3). Next series of simulations focuses on evaluating initial parameters, such as the volcanic plume height of injection (Table 4). Finally, we have evaluated the plume chemistry sensitivity to transport modelling parameters, comparing two vertical advection schemes. These schemes are described and tested in Lachatre et al. (2020b), however, the aforementioned article did not analyze their impact on the chemistry of the modelled plume.

Simulations underlined and labelled "Background" in Table 2,3,4,5 are simulations carried out without emissions originating from volcanic events; while they do not appear in figures themselves, these simulations are necessary to separate background information from our other sensitivity tests. In addition, to better understand the impact of ambient conditions alone on volcanic SO_2 and $SO_{4(p)}^{2-}$ production, "Dry" simulations have been conducted in several cases. These simulations only include SO_2 as volcanic emissions; neither volcanic water nor metals are considered in these cases. For better readability of the results, a unique simulation labelled "Reference" is retained in every panel of simulations. A table describing all the simulation was added in appendix in Table A1 along with the Figure A2 who sums up experiments' results.

3   Results and Discussion

3.1   Reference simulation compared to IASI instrument

The background simulation has been used to exclude non-volcanic information from the Reference simulation and compare to the time-step surrounding IASI sounding for SO_2 (Figure 1). ~~Although we have limited data , it is possible to extract several useful information from the comparison of IASI observations and CHIMERE simulations. Although the positioning~~

Comparison of model outputs with satellite data from the IASI instrument (Figure 1) reveal that several aspects of the simulation outputs are consistent with observations. First, the general shape of the plume ~~on the simulation grid is not accurate in the simulations, other aspects of it, such as its thin shape and~~ , with a NW-SE orientation, fits the observations. The range of values for SO_2 columns is also consistent as well as their structure, with weaker values in the southern part of the plume (around or below $2 \times 10^{17} \mathrm{molec\,cm^{-2}}$) and stronger values (above $5 \times 10^{17} \mathrm{molec\,cm^{-2}}$). Differences are also visible: the plume as represented by CHIMERE is shifted to the North and to the East compared to the ~~concentration gradient seem to match the observations. These characteristics can be used to assess the quality of emissions data, while the small discrepancies seen in the horizontal localisation~~ plume as observed by IASI and the modelled plume extends further towards the southwest, which is not visible in the satellite data. Due to the lack of spatial continuity of the IASI data, it seems difficult to estimate a global mass of SO_2 in the plume. All in all, comparision with IASI data (Figure 1) confirms a correct localization and shape of the plume ~~can be linked to various parameters (meteorological fields,~~ in CHIMERE (but with a horizontal offset of a few hundred kilometers), which is an indirect indication that the plume injection height ~~, transport modelling scheme).~~ in the model is correct: due to substantial wind shear in the troposphere, a large error in the injection height would result in a larger error in the position of the plume.
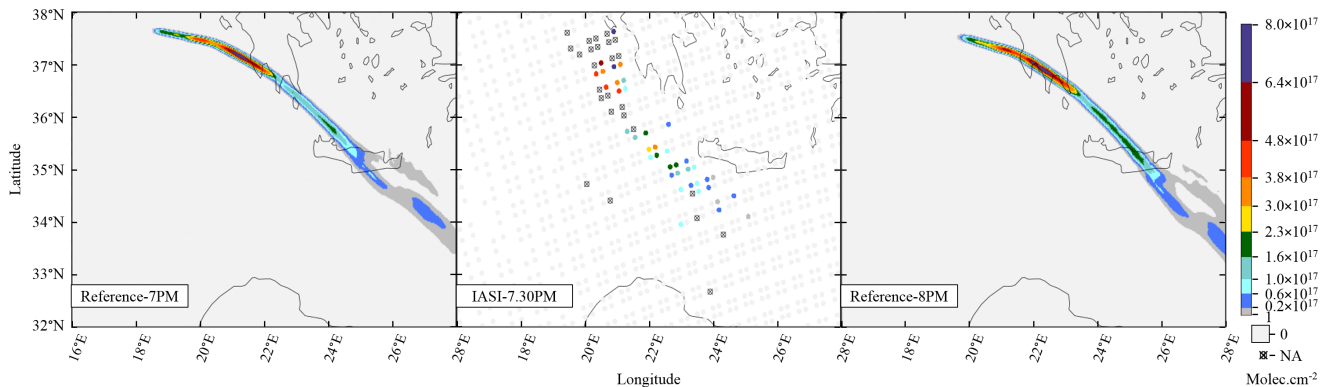
Figure 1. Columns of SO_2 from CHIMERE simulations and IASI measurements. IASI NAs data are shown as a crossed circle. Null values are shown in light gray. IASI sounding corresponds to 7.30PM UTC (center). CHIMERE Reference simulation is displayed for 7PM (left) and 8PM UTC (right).

3.2 Sensitivity tests for chemistry parameters

Table 2. Table gathering simulation parameters for sensitivity tests on chemistry parameters. Underlined items indicate background simulations that are used to retrieve background values. "Volcanic TM" stands for "Volcanic Transition Metals". "No SCLW stands" for "No Super Cooled Liquid Water", No TM_{aq} stands for "No Transition Metals in aqueous phase". The Reference simulation is the closest to a realistic case.

Sensitivity tests on chemistry parameters					
Simulation label	Volcanic SO_2	Volcanic H_2O	Volcanic TM	Volcanic clouds	Injection height	Verticaltransport scheme
Background Background	0.0 kt	0.0 kt	0.0 t	Not applicable	Not applicable	DL99
Dry	8.6 kt	0.0 kt	0.0 t	Not applicable	8.0 km.a.s.l.	DL99
No SCLW	8.6 kt	725.6 kt	0.0 t	Not activated	8.0 km.a.s.l.	DL99
No TM_{aq}	8.6 kt	725.6 kt	0.0 t	Activated	8.0 km.a.s.l.	DL99
Reference	8.6 kt	725.6 kt	7.4 t	Activated	8.0 km.a.s.l.	DL99

In the first group of tests (Table 2), the objective is to estimate the impact of various chemical pathways of SO_2 conversion. As mentioned in Section 2.6, Background and Dry simulations have also been conducted. For these simulations, since volcanic water is not emitted, super cooled water cannot be formed in the model; therefore, the table has been filled with "not applicable" for relevant cases (e.g. volcanic clouds). The simulation No SCLW is slightly different. In this simulation, volcanic water is emitted, but SCLW is not formed from this water, therefore only the additional water vapour from the volcanic water is considered in the model chemistry and only gaseous pathway is evaluated. The next experiment, labelled as No TM_{aq} (No Transition Metals in aqueous phase) is to evaluate the SO_2 conversion into liquid phase, without considering the pathway of oxidation

by O_2 and catalyzed by Fe and Mn; this is presented by Galeazzo et al. (2018) to be the main pathway of $SO_{4(p)}^{2-}$ production. The Reference simulation is considered to be the most realistic simulation performed in this work, in which SO_2 emissions are set to 8.6 kt, H_2O emissions to 725.6 kt, transition metals emissions to 7.4 kt, volcanic super cooled liquid water clouds are activated, mean injection height set to 8.0 km and the vertical transport scheme from Després and Lagoutière (1999) is used.

Figure 2 summarizes the results of simulations conducted in Table 2. Figure 2 shows the hourly evolution of a) the volcanic sulphates mass, b) of volcanic SCLW, ~~d~~c) the minimum volume containing 25 % of $SO_{4(p)}^{2-}$ mass ~~, e~~and d) consequently, the AOD corresponding to the plume following the volume selection~~and e) the mass of hydroxyl radical~~. It can be seen that when volcanic water is added (simulations No $TM_{(aq)}$; Reference) SCLW is formed in the mid-troposphere which is a necessary element to evaluate aqueous chemistry paths. The Dry simulation allows us to evaluate the production of sulphates from reaction to background OH, and appears to be the main oxidation pathway in our experiment (70 %). The addition of volcanic water vapour without formation of SCLW did not significantly increase the conversion of SO_2 to $SO_{4(p)}^{2-}$. The same can be said about the addition of SCLW without TM (No $TM_{(aq)}$ simulation). However, the Reference simulation, which includes volcanic TM significantly increases the conversion of SO_2 (25 %). This additional formation of $SO_{4(p)}^{2-}$ is produced in a very small volume containing the volcanic cloud, which significantly change the optical properties of the plume (and eventually its radiative forcing generated) as it is shown by the evolution of plume's AOD. The comparison of the simulations conducted to ~~understands~~ understand the impact of the various chemical pathways has shown that the conversion of SO_2 mainly occurs in gas phase from reaction with the ambient OH (70 %) and then as a second pathway from the oxidation with O_2 catalyzed by TM in the aqueous phase (25 %).
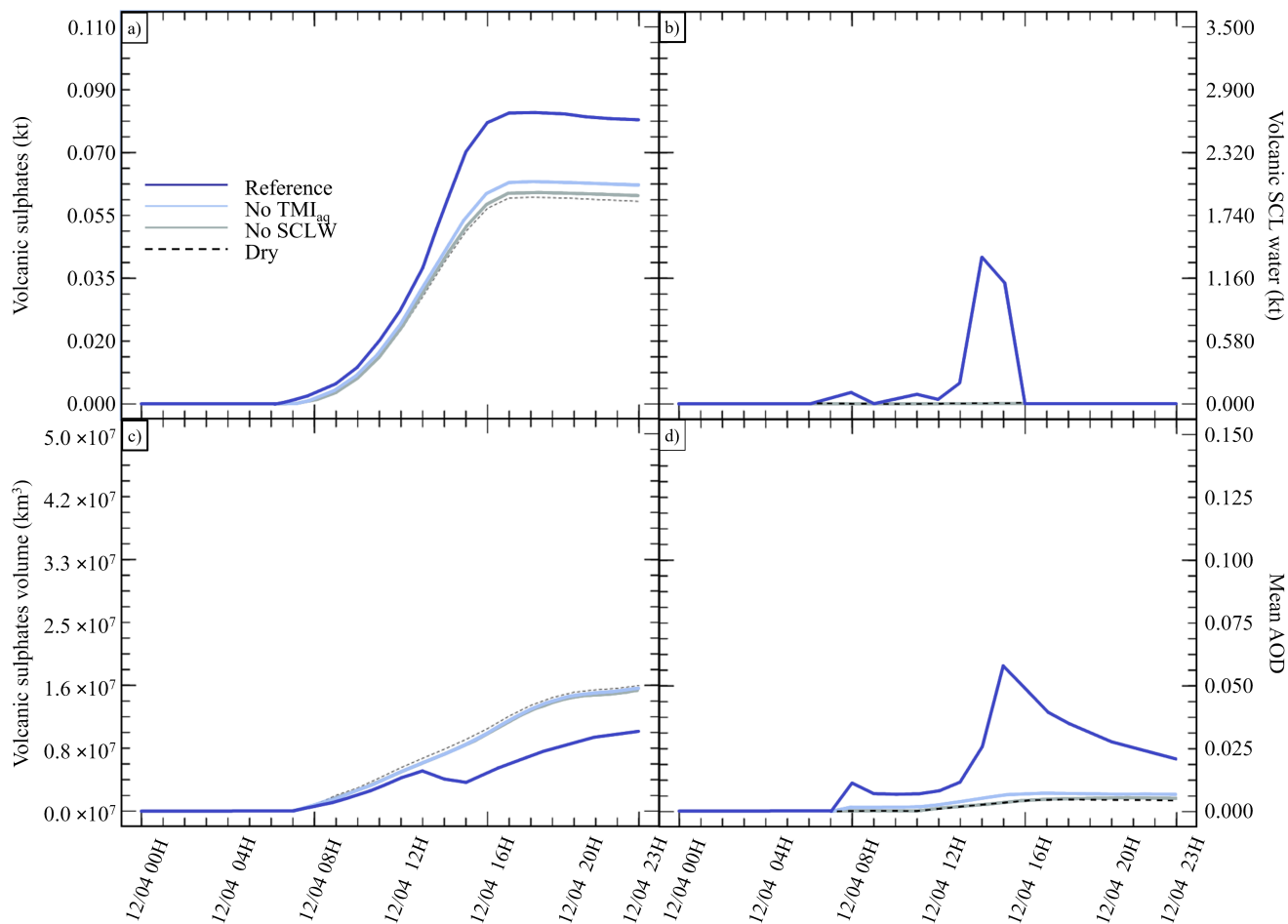
Figure 2. Sensitivity tests on ~~vertical transport scheme~~chemistry parameters. a) Sulphate aerosols (SO$_{4(P)}^{2-}$, kt), b) ~~SCLW~~ Super Cooled Liquid Water (~~kt~~kt), c) ~~AOD for plume~~ Minimum volume (km^3) $\subset$ 25 % of SO$_{4(P)}^{2-}$ mass, d) ~~Minimum volume ()~~ AOD for plume $\subset$ 25 % of SO$_{4(P)}^{2-}$ mass~~, e) radical~~. The Reference simulation is the closest to a realistic case. All time series represent differences relative to the Background simulation (simulation without volcanic emissions).

Then, our work focuses on the impact of various volcanic SO$_2$/H$_2$O ratios (Table 3). Our Reference case takes a ratio of 1 molecule of SO$_2$ per 300 molecules of H$_2$O emitted, thus 725.6 kt of H$_2$O and 8.6 kt of SO$_2$. Two additional cases have been tested with volcanic SO$_2$/H$_2$O ratios of 1/200 and 1/400, corresponding to 483.7 kt and 967.5 kt, and labelled WV200 and WV400 respectively. The aforementioned ratios are considered as threshold values for paroxysmal eruptions. The water apportionment between its various physical states is displayed on Figure A1, in the appendix. Figure 3 summarizes the results of simulations conducted in Table 3. As the cloud generation is a threshold process, the amount of SCLW from volcanic eruption is not linearly linked to the volcanic water vapour emissions. In the WV300 scenario 1.3 kt$_{SCLW}$ is formed at peak time interval (around 12/04 at 12h), against 2.9 kt$_{SCLW}$ and 0.5 kt$_{SCLW}$ in the WV400 and WV200 scenarios respectively. The

Table 3. Table gathering simulation parameters for sensitivity tests on volcanic water emissions. Underlined items indicate background simulations that are used to retrieve background values. "Volcanic TM" stands for "Volcanic Transition Metals". WV200 stands for "Water vapor 200" (mass mixing ratio of 200 to 1 between water vapor and SO_2), and similar acronyms for WV300 and WV400. The Reference simulation is the closest to a realistic case.

	Sensitivity tests on volcanic water emissions					
Simulation label	Volcanic SO_2	Volcanic H_2O	Volcanic TM	Volcanic clouds	Injection height	Vertical transport scheme
~~Background~~ Background	0.0 kt	0.0 kt	0.0 t	Not applicable	Not applicable	DL99
Dry	8.6 kt	0.0 kt	0.0 t	Not applicable	8.0 km.a.s.l.	DL99
WV200	8.6 kt	483.7 kt	7.4 t	Activated	8.0 km.a.s.l.	DL99
Reference (WV300)	8.6 kt	725.6 kt	7.4 t	Activated	8.0 km.a.s.l.	DL99
WV400	8.6 kt	967.5 kt	7.4 t	Activated	8.0 km.a.s.l.	DL99

formation of sulphate with WV400 is 80 % stronger than in the simulation with no volcanic water, and 40% stronger than in the simulation with WV200. This results in an increase of sulphates production; however, this is not a linear process either since the concentrations of SO_2 and the TM are different in the aqueous phase in each of the three cases. Thus, the amount of volcanic water impacts the optical properties of the plume, as the plume's AOD significantly increases following SCLW mass. This aspect is highlighted in the Figure 4 , which displays AOD spatial distribution and summarizes what is shown in Figure 3c-d for the 200 nm AOD.
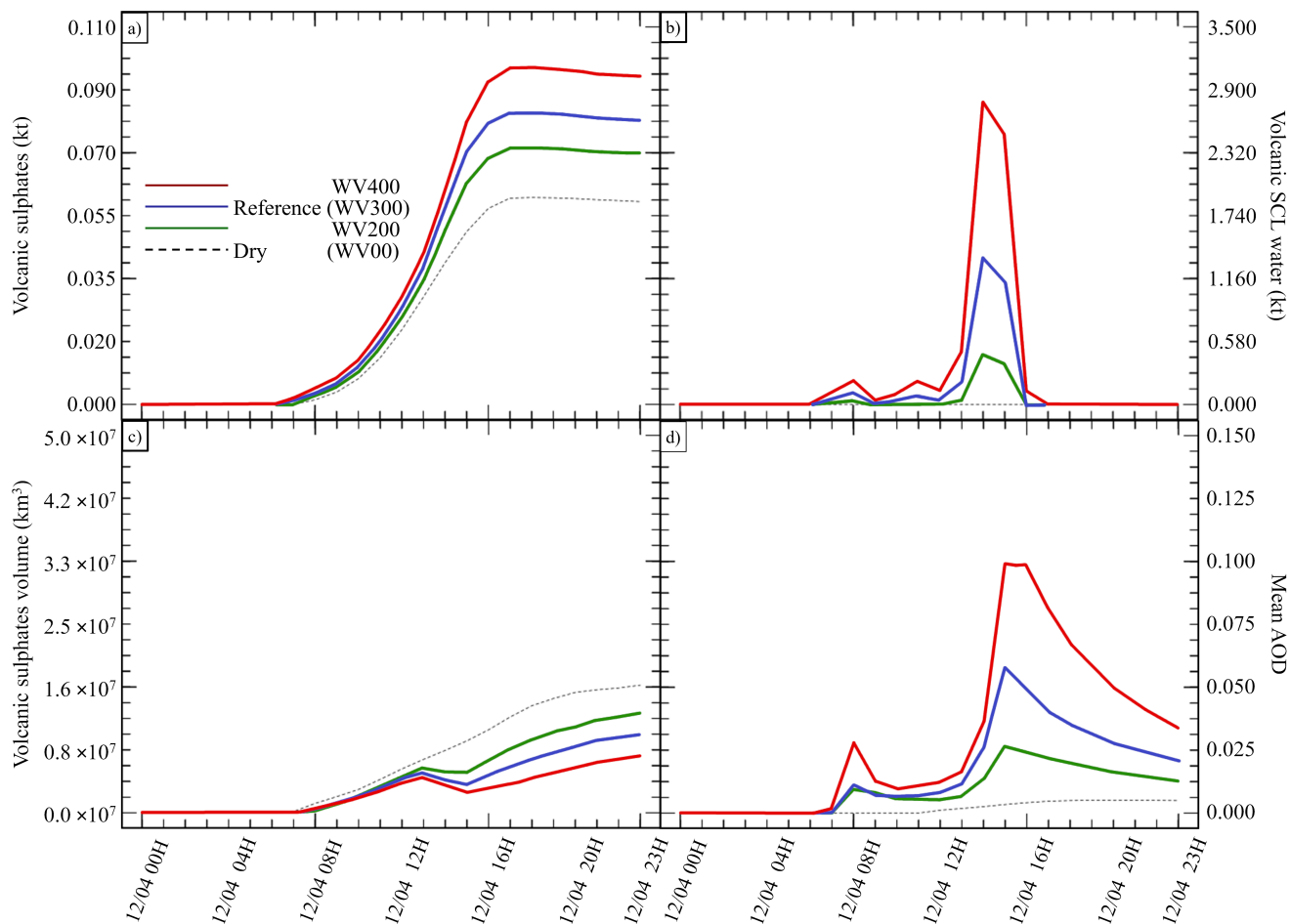
Figure 3. Sensitivity tests on ~~vertical transport schemes~~ volcanic water emissions. a) Sulphate aerosols ($SO_{4(P)}^{2-}$, kt), b) ~~SCLW~~ Super Cooled Liquid Water (kt), c) ~~AOD for plume~~ Minimum volume (km^3) $\subset$ 25 % of $SO_{4(P)}^{2-}$ mass, d) ~~Minimum volume ()~~ AOD for plume $\subset$ 25 % of $SO_{4(P)}^{2-}$ mass~~, e) radical~~. The Reference simulation is the closest to a realistic case. All time series represent differences relative to the Background simulation (simulation without volcanic emissions).

Next, to evaluate the impact of the surrounding environment (Table 4), we have conducted sensitivity tests on the plume's injection height. In our reference simulation, the plume injection is centered around 8.0 km.a.s.l.. A sensitivity test with the injection centered around 8.5 km.a.s.l. has been realized. This second test will provide an environment with a lower atmospheric pressure, lower temperature, dryer atmosphere and different wind speed and direction. Figure 5 summarizes the results of simulations described in Table 4. Comparing simulations Dry 8.0 km and Dry 8.5 km show differences in the results. In the Dry 8.5 km case, less SCLW is generated because of lower humidity, nonetheless more SO_2 are converted to sulphates. This is explained by the higher diffusion of the plume at higher altitude, as it can be seen that the minimum volume occupied by 25 %
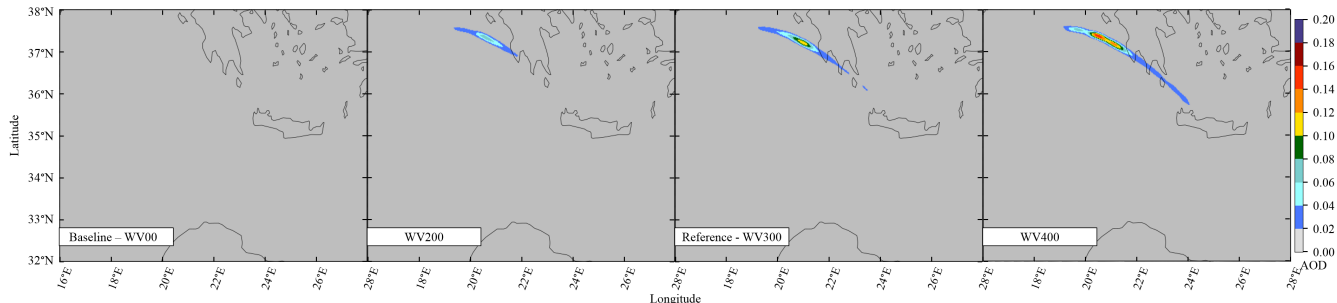
Figure 4. CHIMERE modelled 200 nm AOD from Volcanic sulphates.

Table 4. Table gathering simulation parameters for sensitivity tests on injection height. Underlined items indicate background simulations that are used to retrieve background values. "Volcanic TM" stands for "Volcanic Transition Metals".

		Sensitivity tests on injection height				
Simulation label	Volcanic SO_2	Volcanic H_2O	Volcanic TM	Volcanic clouds	Injection height	Vertical transport scheme
Background	0.0 kt	0.0 kt	0.0 t	Not applicable	Not applicable	DL99
Dry	8.6 kt	0.0 kt	0.0 t	Not applicable	8.0 km.a.s.l.	DL99
Reference	8.6 kt	725.6 kt	7.4 t	Activated	8.0 km.a.s.l.	DL99
~~D.~~**Dry 8.5 km**	8.6 kt	0.0 kt	0.0 t	Not applicable	8.5 km.a.s.l.	DL99
~~R.~~**Reference 8.5 km**	8.6 kt	725.6 kt	7.4 t	Activated	8.5 km.a.s.l.	DL99

of the sulphate mass is bigger than in the Dry 8.0 km. Consequently, this higher dispersion allows a more efficient conversion from OH which is the limiting reactant in the gas phase oxidation.
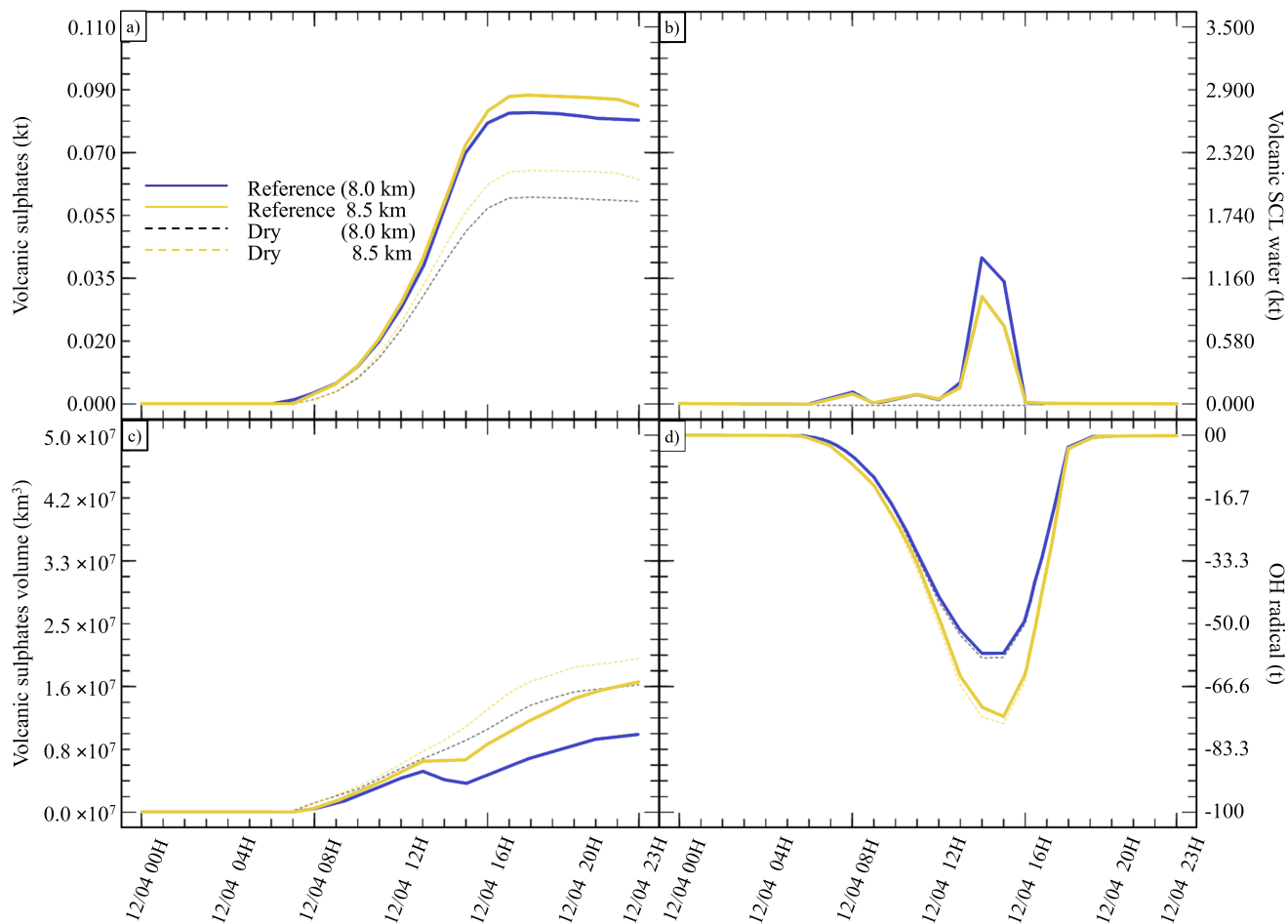
Figure 5. Sensitivity tests on ~~vertical transport scheme~~ injection height. a) Sulphate aerosols (SO$_{4(p)}^{2-}$, kt), b) ~~SCLW~~ Super Cooled Liquid Water (kt), c) ~~AOD for plume ⊂ 25 % of mass, d)~~ Minimum volume (km^3) ⊂ 25 % of SO$_{4(p)}^{2-}$ mass, ~~e~~d) OH radical (t). The Reference simulation is the closest to a realistic case. All time series represent differences relative to the Background simulation (simulation without volcanic emissions).

Finally, we investigate the impact of the plume dispersion on the computed chemistry (Table 5). Following the work done in Lachatre et al. (2020b) on different transport schemes, the Reference simulations has been conducted with the Després and Lagoutière (1999) vertical transport scheme (DL99), reducing the excessive plume diffusion that has been observed in previous work (Colette et al., 2011; Boichu et al., 2013; Lachatre et al., 2020a). In comparison, simulations with the Van Leer (1977) (VL77) vertical transport scheme have been conducted; this transport scheme being expected to induce a larger spreading of the volcanic plume. For this last case, it was necessary to compute again a background simulation, using the VL77 vertical transport scheme.

Figure 6 summarizes the results of simulations conducted in Table 5. It was expected to see a larger spread of the plume in the

Table 5. Table gathering simulation parameters for sensitivity tests on vertical transport scheme. Underlined items indicate background simulations that are used to retrieve background values. "Volcanic TM" stands for "Volcanic Transition Metals". "Background VL" stands for "Background with the Van Leer (1977) advection scheme; "Background VL" stands for "Dry with the Van Leer (1977) advection scheme; "Reference VL" stands for "Reference with the Van Leer (1977) advection scheme.

Sensitivity tests on vertical transport scheme						
Simulation label	Volcanic SO_2	Volcanic H_2O	Volcanic TM	Volcanic clouds	Injection height	Vertical transport scheme
Background	0.0 kt	0.0 kt	0.0 t	Not applicable	Not applicable	DL99
Dry	8.6 kt	0.0 kt	0.0 t	Not applicable	8.0 km.a.s.l.	DL99
Reference	8.6 kt	725.6 kt	7.4 t	Activated	8.0 km.a.s.l.	DL99
~~Background VL~~ **Background VL**	0.0 kt	0.0 kt	0.0 t	Not applicable	Not applicable	VL77
~~D.~~**Dry** VL	8.6 kt	0.0 kt	0.0 t	Not applicable	8.0 km.a.s.l.	VL77
~~R.~~**Reference** VL	8.6 kt	725.6 kt	7.4 t	Activated	8.0 km.a.s.l.	VL77

sensitivity test with VL77 compared to the Reference simulation using the Després and Lagoutière (1999) vertical advection scheme. Indeed, the volume of the plume has significantly increased, as it is displayed on Figure 6~~d~~c). Consequently, less SCLW has been generated, but on the other hand, more sulphates were produced. This is due to higher conversion from the ambient OH, as it can be seen that more radical has been consumed (Figure 6~~e~~d). It can also be noted that Reference VL's AOD is lower than Reference DL's AOD, due to the significantly larger spreading of Reference VL plume. This result was slightly unexpected as gaseous oxidation appeared to be linear at first; still, this new observation makes sense since more OH were mobilized to react with the volcanic SO_2 in excess.
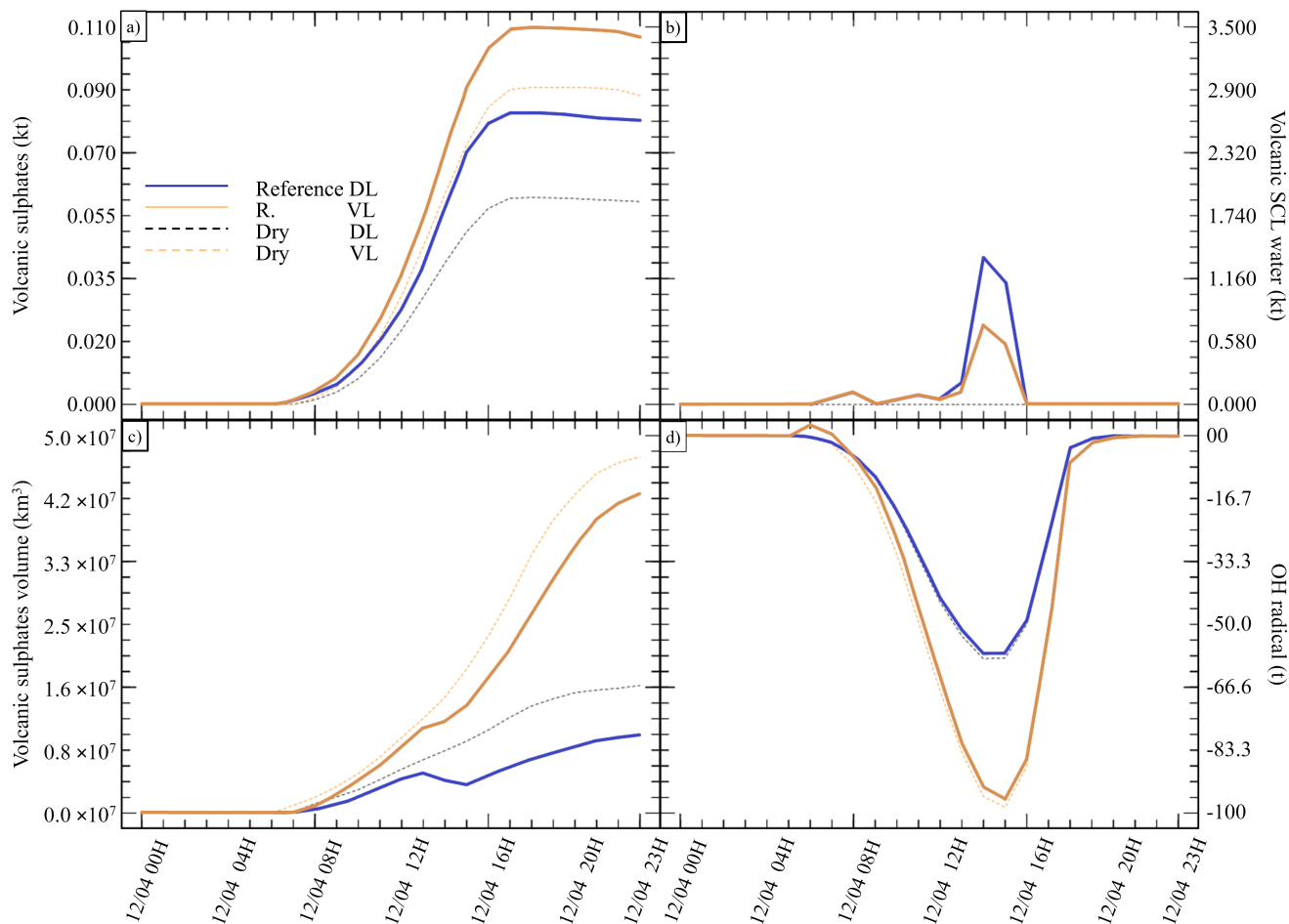
Figure 6. Sensitivity tests on injection height. a) ~~Sulphate aerosols~~ ($SO_{4(p)}^{2-}$, kt), b) ~~SCLW~~ Super Cooled Liquid Water (kt), c) ~~AOD for plume ⊂ 25 % of mass, d)~~ Minimum volume (km^3) ⊂ 25 % of $SO_{4(p)}^{2-}$ mass, ~~e~~d) OH radical (t). The Reference simulation is the closest to a realistic case. All time series represent differences relative to the Background simulation (simulation without volcanic emissions).

4   Conclusions

In this study we aimed to investigate volcanic plume chemistry in the mid-troposphere region using the CHIMERE CTM. With the assistance of the IASI instrument's SO_2 sounding, we have determined that the CHIMERE model is able to reproduce a realistic structure for the plume as well as a correct intensity in terms of SO_2 columns after a number of assumptions were made. Because of these encouraging preliminary observations, we gained confidence in the subsequent results. We have then analyzed the impact of various oxidation pathways by selectively shutting down these pathways to evaluate their contribution. For our study case, these sensitivity tests suggest that the main oxidation pathway is gas-phase oxidation by OH (about 70 %),

followed by liquid-phase catalyzed oxidation by O_2 (about 25%). The fact that liquid-phase oxidation is dominated by TM-catalyzed oxidation is in line with the results of Galeazzo et al. (2018), and confirms that, unlike what typically happens in polluted plumes, in such a volcanic plume availability of H_2O_2 rapidly becomes insufficient to substantially contribute to SO_2 oxidation. Therefore, our conclusion is that this oxidation pathway should be included in all modelling studies dealing with aqueous oxidation of volcanic SO_2. ~~Our results calls for better constraining the quantities of dissolved and in volcanic cloud water through field measurements and further experimental studies.~~

We have tested the impact of H_2O/SO_2 ratio, with four hypotheses: No volcanic water, $H_2O/SO_2 = 200/1$, 300/1, and 400/1. These tests confirm that, depending on the H_2O/SO_2 ratio and on the background atmospheric condition, the presence and quantity of volcanic water vapour potentially has a strong impact on sulphate formation: in our case study, the formation of sulphate with $H_2O/SO_2 = 400/1$ is 80 % stronger than in the simulation with no volcanic water, and 40% stronger than in the simulation with $H_2O/SO_2 = 200/1$; therefore, in some cases such as mid-tropospheric plumes, including volcanic water may be necessary to correctly represent the conversion of volcanic SO_2 into sulphate aerosols. Apart from the above-mentioned change in the overall quantity of sulphates formed, the localized formation of a liquid-containing volcanic plume may generate strong maxima in the sulphate AOD ($\sim$0.1 in our case study), while in the case devoid of volcanic water sulphate AOD never exceeds $\sim$0.005, far from any instrumental detection threshold. These sensitivity tests suggest the strong sensitivity of liquid-phase SO_2 oxidation to the injection height of the plume: if the plume is too low, then due to warm ambient temperature, volcanic water input may not be sufficient to reach saturation, but if the plume is too high, temperatures will be too cold to permit the formation of a liquid aqueous phase. Therefore, our conclusion on the strong sensitivity of SO_2 oxidation to the H_2O/SO_2 ratio may hold only for mid-tropospheric plumes such as the one in our case study. This does not mean that the impact of volcanic water on chemistry is not relevant at higher altitudes: on the contrary, the influence of gas-phase volcanic water vapour may still be of interest in the case of upper tropospheric or stratospheric plumes, where an additional input of water vapour would enhance the formation of the OH.

Apart from the sensitivity to uncertainties concerning the physico-chemical processes and the forcings that we have discussed above, representation of SO_2 oxidation in volcanic plumes is also sensitive to the discretization strategies and to the numerical schemes that are used. For example, our sensitivity tests show that reducing excessive numerical diffusion by using an antidiffusive transport scheme such as Després and Lagoutière (1999) can change the structure of the modelled plume strongly, and in a complex way. In our case, reducing diffusion leads to a reduction in total production of sulphates, but with sharper gradients and stronger peaks in concentration and AOD. Due to chemical nonlinearities (*e.g* the reduced availability of OH in the plume), reducing numerical diffusion can change the quantitative and qualitative properties of the resulting sulphate plume in a much more subtle way than just spreading the plume over a greater volume, as observed in Lachatre et al. (2020b) for an inert tracer. This confirms that chemistry-transport modellers should pay attention to reduce numerical diffusion in their model, not only because excessive numerical diffusion will affect the spread of the plumes, but also, as we have shown here, because it will affect chemistry in a non-linear way, which in turn affects the AOD and therefore the radiative effect of particles.

This study shows the need to better constrain several parameters that we have shown to be crucial in the representation of the chemical behavior of volcanic plumes in the atmosphere. For example, it is critical to have better observational estimates

of the H_2O/SO_2 ratio in an eruptive context. We also confirm the box-model results of Galeazzo et al. (2018), which suggest that the impact of transition metals in liquid-phase oxidation of volcanic SO_2 is substantial. This highlights the need to better constrain volcanic emissions of Fe(III) and Mn(II) in the atmosphere and their subsequent repartition between volcanic ash and aqueous phase. As it has been shown by Hoshyaripour et al. (2014), emissions of these transition metals can vary greatly among different volcanic environments. Therefore, our results calls for better constraining the quantities of dissolved Fe(III) and Mn(II) in volcanic cloud water through field measurements and further experimental studies. In the case of Mount Etna, this quantification could be performed with more sampling and analyses of their contents in ash and plume samples through use of passive traps. To be comprehensive, this sampling would have to be done ad different distances from the craters, both during passive degassing periods and during eruptions. The present study also highlights the need to find ways to reduce numerical diffusion in chemistry-transport models, through not only using better numerical strategies as shown here, but also by examining other approaches such as adaptative mesh refinement in both the horizontal and vertical dimensions.

Code and data availability

The source code for the CHIMERE model (Mailler et al., 2017) is available on: https://www.lmd.polytechnique.fr/chimere/. WRF source code is available on: https://github.com/wrf-model/WRF/. Clarisse, L. (2019). Daily IASI/Metop-B ULB-LATMOS sulphur dioxide (SO_2) L2 product (columns and altitude) [Data set]. AERIS. https://doi.org/10.25326/42. SO_2 (Salerno et al., 2018) flux measurement data are available contacting the authors. Simulation outputs are available contacting the authors.

Authors contributions

All of the authors help to design the experiments. G.S. and S.G. provided the volcanic emissions data. A.C. prepared the anthropogenic emissions. S.M., G.S and M.L. adapted the model. M.L. carried out the simulations and prepared the results. M.L. and S.M. prepared the manuscript. All authors contributed to the text, interpretation of the results and reviewed the manuscript.

Acknowledgements. This study has been supported by AID (Agence de l'Innovation de Défense) under grant TROMPET. Simulations have been performed on the Irene supercomputer in the framework of GENCI GEN10274 project. This work has been supported by the Programme National de Télédétection Spatiale (PNTS, http://www.insu.cnrs.fr/pnts), grant n°PNTS-2019-9.

Appendix A: ~~Material~~ Supplementary tables and ~~methods~~figures
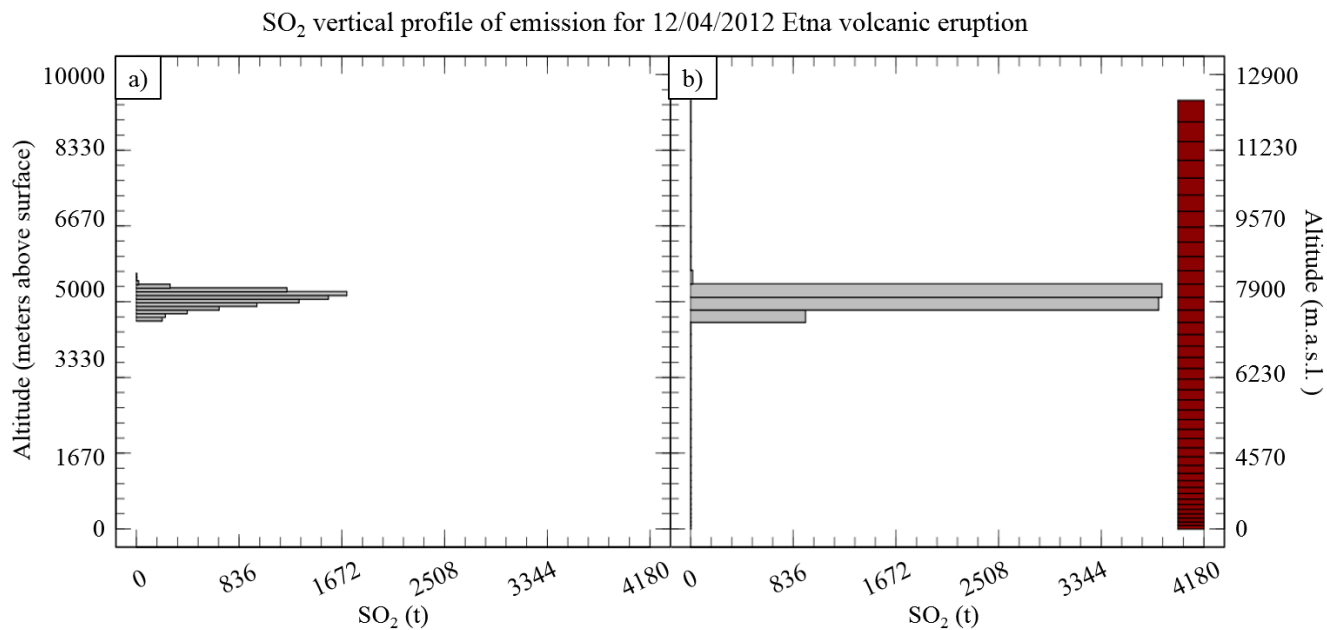
Figure A1. SO$_2$ vertical profile of emission for 12/04/2012 Etna volcanic eruption. a) Emission distribution following a skewed distribution. b) Emissions in the model after adaptation to the vertical grid used in CHIMERE (shown as red boxes).
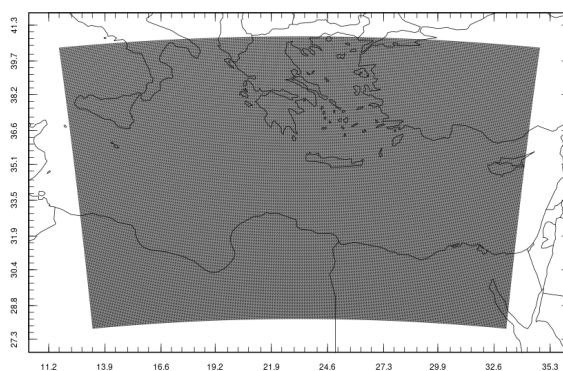
Figure A2. The CHIMERE simulation domain contains 874 × 624 cells at 2.250 km resolution
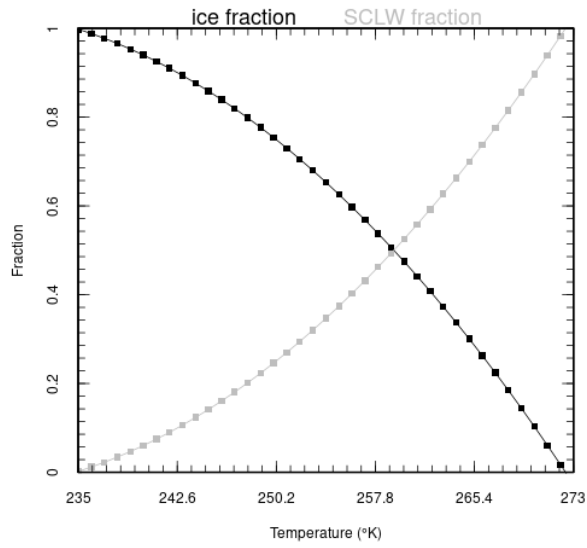
Figure A3. SCLW and ice fraction depending on temperature

Appendix B: ~~Results and Discussion~~
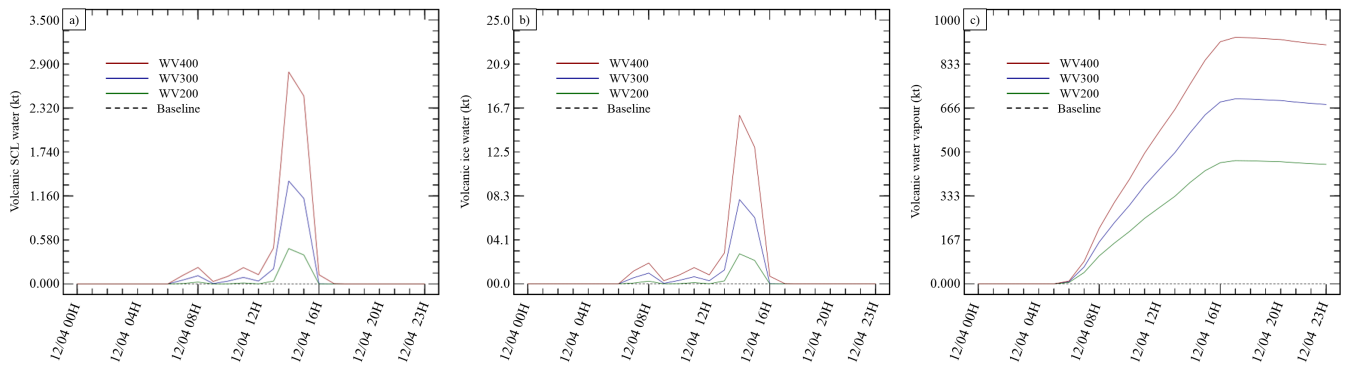
Figure A1. Water apportionment between its various states. a)SCL Water, b) ice, c) water vapour.

Table A1. Synthetic list of the 13 simulations that have been performed for this study and their description

Simulation label	Developed description
Background	Simulates the atmosphere as it would be without a volcanic eruption (no emissions of volcanic SO_2, volcanic water or volcanic transition metals
Dry	Simulates the atmosphere as it would be with emissions of volcanic SO_2 but no emissions of volcanic water or volcanic transition metals
No SCLW	Simulates the atmosphere as it would be with emissions of volcanic SO_2 and of volcanic water but volcanic water is not allowed to contribute to a liquid phase. No emissions of transition metals. "No SCLW" stands for "No Super Cooled Liquid Water"
No TM$_{aq}$	Simulates the atmosphere as it would be with emissions of volcanic SO_2 and of volcanic water. Volcanic water is allowed to contribute to a liquid phase. No emissions of transition metals. "No TM$_{aq}$" stands for "No Transition Metals in Aqueous phase"
Reference	**Reference simulation**, including emissions of volcanic SO_2, volcanic water and volcanic transition metals, and permitting volcanic water to contribute to a liquid phase. The $\frac{H_2O}{SO_2}$ mass emission ratio is set to 300.
WV200	Same as **Reference** but the $\frac{H_2O}{SO_2}$ mass emission ratio is set to 200. "WV200" stands for "Water Vapor 200"
WV400	Same as **Reference** but the $\frac{H_2O}{SO_2}$ mass emission ratio is set to 400. "WV400" stands for "Water Vapor 400"
Dry 8.5 km	Same as **Dry** but the volcanic plume is released at $8500\,\mathrm{m.a.s.l}$ instead of $8000\,\mathrm{m.a.s.l}$
Reference 8.5 km	Same as **Reference** but the volcanic plume is released at $8500\,\mathrm{m.a.s.l}$ instead of $8000\,\mathrm{m.a.s.l}$
Background VL	Same as **Background** but using the Van Leer (1977) advection scheme instead of Després and Lagoutière (1999)
Dry VL	Same as **Dry** but using the Van Leer (1977) advection scheme instead of Després and Lagoutière (1999)
Reference VL	Same as **Reference** but using the Van Leer (1977) advection scheme instead of Després and Lagoutière (1999)
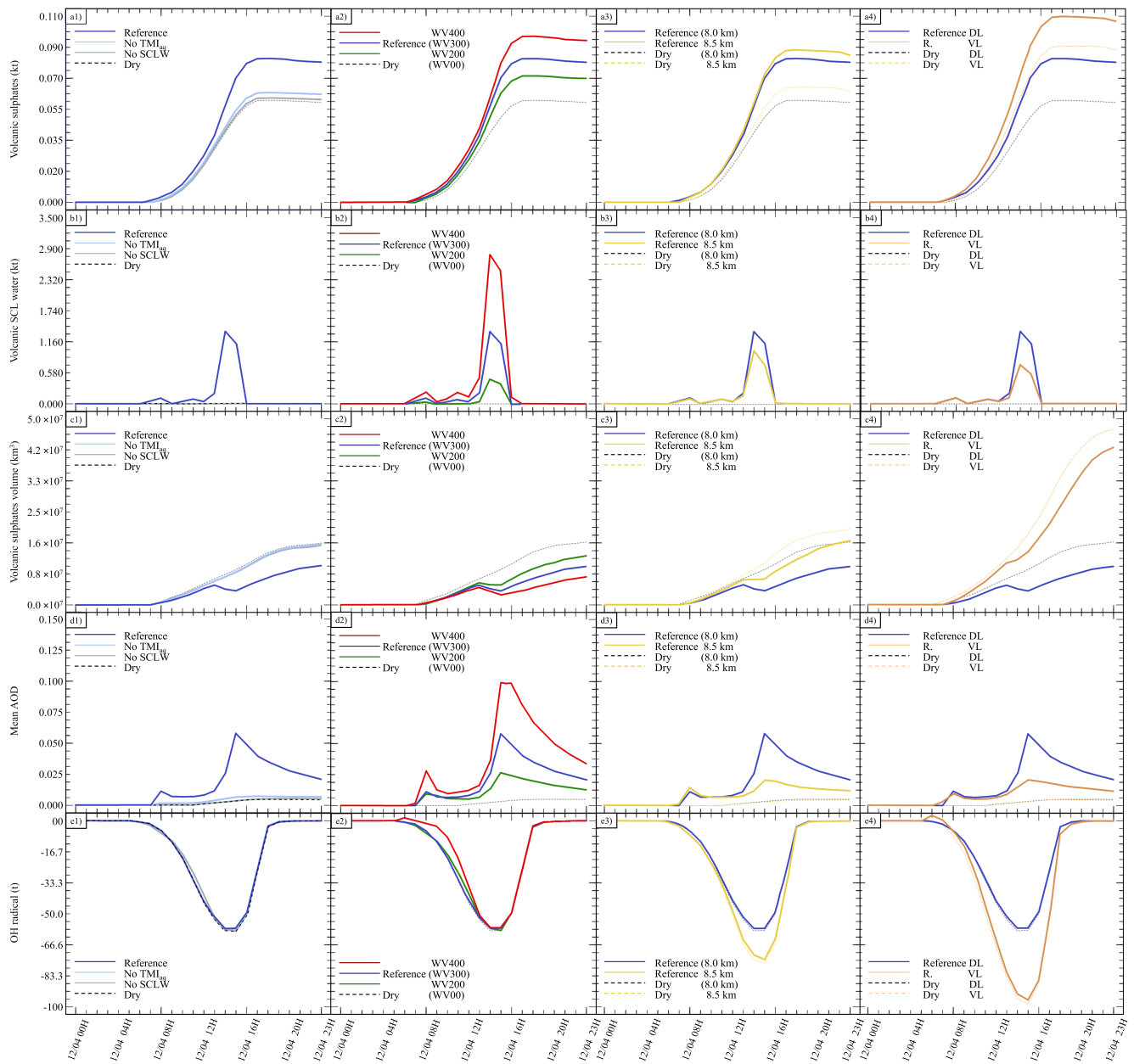
Figure A2. Gathering of the various performed experiences' results. a) $SO_{4(p)}^{2-}$ (kt), b) Super Cooled Liquid Water (kt), c) Minimum volume (km^3) $\subset$ 25 % of $SO_{4(p)}^{2-}$ mass, d) AOD for plume $\subset$ 25 % of $SO_{4(p)}^{2-}$ mass and e) OH radical (t). The Reference simulation is the closest to a realistic case.

References

Ayris, P. and Delmelle, P.: Volcanic and atmospheric controls on ash iron solubility: A review, Physics and Chemistry of the Earth, Parts A/B/C, 45-46, 103–112, https://doi.org/https://doi.org/10.1016/j.pce.2011.04.013, https://www.sciencedirect.com/science/article/pii/S1474706511000775, volcanic ash: an agent in Earth systems, 2012.

Bian, H. and Prather, M. J.: Fast-J2: Accurate Simulation of Stratospheric Photolysis in Global Chemical Models, Journal of Atmospheric Chemistry, 41, 281–296, https://doi.org/10.1023/A:1014980619462, https://doi.org/10.1023/A:1014980619462, 2002.

Boichu, M., Menut, L., Khvorostyanov, D., Clarisse, L., Clerbaux, C., Turquety, S., and Coheur, P.-F.: Inverting for volcanic SO_2 flux at high temporal resolution using spaceborne plume imagery and chemistry-transport modelling: the 2010 Eyjafjallajökull eruption case study, Atmospheric Chemistry and Physics, 13, 8569–8584, https://doi.org/10.5194/acp-13-8569-2013, https://www.atmos-chem-phys.net/13/8569/2013/, 2013.

Briant, R., Tuccella, P., Deroubaix, A., Khvorostyanov, D., Menut, L., Mailler, S., and Turquety, S.: Aerosol–radiation interaction modelling using online coupling between the WRF 3.7.1 meteorological model and the CHIMERE 2016 chemistry-transport model, through the OASIS3-MCT coupler, Geoscientific Model Development, 10, 927–944, https://doi.org/10.5194/gmd-10-927-2017, https://www.geosci-model-dev.net/10/927/2017/, 2017.

Calabrese, S., Aiuppa, A., Allard, P., Bagnato, E., Bellomo, S., Brusca, L., D'Alessandro, W., and Parello, F.: Atmospheric sources and sinks of volcanogenic elements in a basaltic volcano (Etna, Italy), Geochimica et Cosmochimica Acta, 75, 7401–7425, https://doi.org/https://doi.org/10.1016/j.gca.2011.09.040, https://www.sciencedirect.com/science/article/pii/S0016703711005618, 2011.

Carboni, E., Grainger, R., Walker, J., Dudhia, A., and Siddans, R.: A new scheme for sulphur dioxide retrieval from IASI measurements: application to the Eyjafjallajökull eruption of April and May 2010, Atmospheric Chemistry and Physics, 12, 11 417–11 434, https://doi.org/10.5194/acp-12-11417-2012, https://www.atmos-chem-phys.net/12/11417/2012/, 2012.

Carboni, E., Grainger, R. G., Mather, T. A., Pyle, D. M., Thomas, G. E., Siddans, R., Smith, A. J. A., Dudhia, A., Koukouli, M. E., and Balis, D.: The vertical distribution of volcanic SO_2 plumes measured by IASI, Atmospheric Chemistry and Physics, 16, 4343–4367, https://doi.org/10.5194/acp-16-4343-2016, https://www.atmos-chem-phys.net/16/4343/2016/, 2016.

Clarisse, L., Hurtmans, D., Clerbaux, C., Hadji-Lazaro, J., Ngadi, Y., and Coheur, P.-F.: Retrieval of sulfur dioxide from the infrared atmospheric sounding interferometer (IASI), Atmospheric Measurement Techniques, 5, 581–594, https://doi.org/10.5194/amt-5-581-2012, https://amt.copernicus.org/articles/5/581/2012/, 2012.

Clarisse, L., Coheur, P.-F., Theys, N., Hurtmans, D., and Clerbaux, C.: The 2011 Nabro eruption, a SO_2 plume height analysis using IASI measurements, Atmospheric Chemistry and Physics, 14, 3095–3111, https://doi.org/10.5194/acp-14-3095-2014, https://acp.copernicus.org/articles/14/3095/2014/, 2014.

Colette, A., Favez, O., Meleux, F., Chiappini, L., Haeffelin, M., Morille, Y., Malherbe, L., Papin, A., Bessagnet, B., Menut, L., Leoz, E., and Rouïl, L.: Assessing in near real time the impact of the April 2010 Eyjafjallajokull ash plume on air quality, Atmospheric Environment, 45, 1217 – 1221, https://doi.org/https://doi.org/10.1016/j.atmosenv.2010.09.064, http://www.sciencedirect.com/science/article/pii/S1352231010008502, 2011.

Connick, R. E. and Zhang, Y.-X.: Kinetics and Mechanism of the Oxidation of HSO3- by O2. 2. The Manganese(II)-Catalyzed Reaction, Inorganic Chemistry, 35, 4613–4621, https://doi.org/10.1021/ic951141i, https://doi.org/10.1021/ic951141i, 1996.

Derognat, C., Beekmann, M., Baeumle, M., Martin, D., and Schmidt, H.: Effect of biogenic volatile organic compound emissions on tropospheric chemistry during the Atmospheric Pollution Over the Paris Area (ESQUIF) campaign in the Ile-de-France region, Journal

of Geophysical Research: Atmospheres, 108, https://doi.org/https://doi.org/10.1029/2001JD001421, https://agupubs.onlinelibrary.wiley.com/doi/abs/10.1029/2001JD001421, 2003.

Desboeufs, K., Losno, R., and Colin, J.: Factors influencing aerosol solubility during cloud processes, Atmospheric Environment, 35, 3529–3537, https://doi.org/https://doi.org/10.1016/S1352-2310(00)00472-6, https://www.sciencedirect.com/science/article/pii/S1352231000004726, 2001.

Després, B. and Lagoutière, F.: Un schéma non linéaire anti-dissipatif pour l'équation d'advection linéaire, Comptes Rendus de l'Académie des Sciences - Series I - Mathematics, 328, 939 – 943, https://doi.org/https://doi.org/10.1016/S0764-4442(99)80301-2, http://www.sciencedirect.com/science/article/pii/S0764444299803012, 1999.

Eckhardt, S., Prata, A. J., Seibert, P., Stebel, K., and Stohl, A.: Estimation of the vertical profile of sulfur dioxide injection into the atmosphere by a volcanic eruption using satellite column measurements and inverse transport modeling, Atmospheric Chemistry and Physics, 8, 3881–3897, https://doi.org/10.5194/acp-8-3881-2008, https://acp.copernicus.org/articles/8/3881/2008/, 2008.

Galeazzo, T., Bekki, S., Martin, E., Savarino, J., and Arnold, S. R.: Photochemical box modelling of volcanic SO_2 oxidation: isotopic constraints, Atmospheric Chemistry and Physics, 18, 17 909–17 931, https://doi.org/10.5194/acp-18-17909-2018, https://www.atmos-chem-phys.net/18/17909/2018/, 2018.

Ginoux, P., Chin, M., Tegen, I., Prospero, J. M., Holben, B. adn Dubovik, O., and Lin, S.: Sources and distributions of dust aerosols simulated with the GOCART model, Journal of Geophysical Research : Atmospheres, 2001.

Guermazi, H., Sellitto, P., Cuesta, J., Eremenko, M., Lachatre, M., Mailler, S., Carboni, E., Salerno, G., Caltabiano, T., Menut, L., Serbaji, M. M., Rekhiss, F., and Legras, B.: Quantitative Retrieval of Volcanic Sulphate Aerosols from IASI Observations, Remote Sensing, 13, https://doi.org/10.3390/rs13091808, https://www.mdpi.com/2072-4292/13/9/1808, 2021.

Hauglustaine, D. A., Hourdin, F., Jourdain, L., Filiberti, M.-A., Walters, S., Lamarque, J.-F., and Holland, E. A.: Interactive chemistry in the Laboratoire de Météorologie Dynamique general circulation model: Description and background tropospheric chemistry evaluation, Journal of Geophysical Research: Atmospheres, 109, https://doi.org/https://doi.org/10.1029/2003JD003957, https://agupubs.onlinelibrary.wiley.com/doi/abs/10.1029/2003JD003957, 2004.

Heard, I. P. C., Manning, A. J., Haywood, J. M., Witham, C., Redington, A., Jones, A., Clarisse, L., and Bourassa, A.: A comparison of atmospheric dispersion model predictions with observations of SO2 and sulphate aerosol from volcanic eruptions, Journal of Geophysical Research: Atmospheres, 117, https://doi.org/10.1029/2011JD016791, 2012.

Hoshyaripour, G., Hort, M., Langmann, B., and Delmelle, P.: Volcanic controls on ash iron solubility: New insights from high-temperature gas–ash interaction modeling, Journal of Volcanology and Geothermal Research, 286, 67 – 77, https://doi.org/https://doi.org/10.1016/j.jvolgeores.2014.09.005, http://www.sciencedirect.com/science/article/pii/S0377027314002844, 2014.

Hoshyaripour, G. A., Hort, M., and Langmann, B.: Ash iron mobilization through physicochemical processing in volcanic eruption plumes: a numerical modeling approach, Atmospheric Chemistry and Physics, 15, 9361–9379, https://doi.org/10.5194/acp-15-9361-2015, https://www.atmos-chem-phys.net/15/9361/2015/, 2015.

Hu, Y., Rodier, S., Xu, K.-m., Sun, W., Huang, J., Lin, B., Zhai, P., and Josset, D.: Occurrence, liquid water content, and fraction of supercooled water clouds from combined CALIOP/IIR/MODIS measurements, Journal of Geophysical Research: Atmospheres, 115, https://doi.org/https://doi.org/10.1029/2009JD012384, https://agupubs.onlinelibrary.wiley.com/doi/abs/10.1029/2009JD012384, 2010.

Itahashi, S., Mathur, R., Hogrefe, C., Napelenok, S. L., and Zhang, Y.: Incorporation of volcanic SO_2 emissions in the Hemispheric CMAQ (H-CMAQ) version 5.2 modeling system and assessing their impacts on sulfate aerosol over Northern Hemisphere, Geoscientific Model Development Discussions, 2021, 1–28, https://doi.org/10.5194/gmd-2021-109, 2021.

Janssens-Maenhout, G., Crippa, M., Guizzardi, D., Dentener, F., Muntean, M., Pouliot, G., Keating, T., Zhang, Q., Kurokawa, J., Wankmüller, R., Denier Van Der Gon, H., Kuenen, J. J. P., Klimont, Z., Frost, G., Darras, S., Koffi, B., and Li, M.: HTAP-v2.2: A mosaic of regional and global emission grid maps for 2008 and 2010 to study hemispheric transport of air pollution, Atmospheric Chemistry and Physics, 15, 11 411–11 432, https://doi.org/10.5194/acp-15-11411-2015, 2015.

Jourdain, L., Roberts, T. J., Pirre, M., and Josse, B.: Modeling the reactive halogen plume from Ambrym and its impact on the troposphere with the CCATT-BRAMS mesoscale model, Atmospheric Chemistry and Physics, 16, 12 099–12 125, https://doi.org/10.5194/acp-16-12099-2016, https://acp.copernicus.org/articles/16/12099/2016/, 2016.

Kloss, C., Berthet, G., Sellitto, P., Ploeger, F., Taha, G., Tidiga, M., Eremenko, M., Bossolasco, A., Jégou, F., Renard, J.-B., and Legras, B.: Stratospheric aerosol layer perturbation caused by the 2019 Raikoke and Ulawun eruptions and their radiative forcing, Atmospheric Chemistry and Physics, 21, 535–560, https://doi.org/10.5194/acp-21-535-2021, https://acp.copernicus.org/articles/21/535/2021/, 2021.

Komurcu, M., Storelvmo, T., Tan, I., Lohmann, U., Yun, Y., Penner, J. E., Wang, Y., Liu, X., and Takemura, T.: Intercomparison of the cloud water phase among global climate models, Journal of Geophysical Research: Atmospheres, 119, 3372–3400, https://doi.org/https://doi.org/10.1002/2013JD021119, https://agupubs.onlinelibrary.wiley.com/doi/abs/10.1002/2013JD021119, 2014.

Kärcher, B. and Seifert, A.: On homogeneous ice formation in liquid clouds, Quarterly Journal of the Royal Meteorological Society, 142, 1320–1334, https://doi.org/10.1002/qj.2735, https://rmets.onlinelibrary.wiley.com/doi/abs/10.1002/qj.2735, 2016.

Lachatre, M., Foret, G., Laurent, B., Siour, G., Cuesta, J., Dufour, G., Meng, F., Tang, W., Zhang, Q., and Beekmann, M.: Air Quality Degradation by Mineral Dust over Beijing, Chengdu and Shanghai Chinese Megacities, Atmosphere, 11, https://doi.org/10.3390/atmos11070708, https://www.mdpi.com/2073-4433/11/7/708, 2020a.

Lachatre, M., Mailler, S., Menut, L., Turquety, S., Sellitto, P., Guermazi, H., Salerno, G., Caltabiano, T., and Carboni, E.: New strategies for vertical transport in chemistry transport models: application to the case of the Mount Etna eruption on 18 March 2012 with CHIMERE v2017r4, Geoscientific Model Development, 13, 5707–5723, https://doi.org/10.5194/gmd-13-5707-2020, https://gmd.copernicus.org/articles/13/5707/2020/, 2020b.

Lagrange, J., Pallares, C., and Lagrange, P.: Electrolyte effects on aqueous atmospheric oxidation of sulphur dioxide by ozone, Journal of Geophysical Research: Atmospheres, 99, 14 595–14 600, https://doi.org/https://doi.org/10.1029/94JD00573, https://agupubs.onlinelibrary.wiley.com/doi/abs/10.1029/94JD00573, 1994.

Langmann, B.: On the Role of Climate Forcing by Volcanic Sulphate and Volcanic Ash, Advances in Meteorology, p. Article ID 340123, https://doi.org/https://doi.org/10.1155/2014/340123, 2014.

Mailler, S., Menut, L., di Sarra, A. G., Becagli, S., Di Iorio, T., Bessagnet, B., Briant, R., Formenti, P., Doussin, J.-F., Gómez-Amo, J. L., Mallet, M., Rea, G., Siour, G., Sferlazzo, D. M., Traversi, R., Udisti, R., and Turquety, S.: On the radiative impact of aerosols on photolysis rates: comparison of simulations and observations in the Lampedusa island during the ChArMEx/ADRIMED campaign, Atmospheric Chemistry and Physics, 16, 1219–1244, https://doi.org/10.5194/acp-16-1219-2016, https://acp.copernicus.org/articles/16/1219/2016/, 2016.

Mailler, S., Menut, L., Khvorostyanov, D., Valari, M., Couvidat, F., Siour, G., Turquety, S., Briant, R., Tuccella, P., Bessagnet, B., Colette, A., Létinois, L., Markakis, K., and Meleux, F.: CHIMERE-2017: From urban to hemispheric chemistry-transport modeling, Geoscientific Model Development, 10, 2397–2423, https://doi.org/10.5194/gmd-10-2397-2017, 2017.

Mailler, S., Pennel, R., Menut, L., and Lachâtre, M.: Using an antidiffusive transport scheme in the vertical direction: a promising novelty for chemistry-transport models, Geoscientific Model Development, 2020, 1–21, https://doi.org/10.5194/gmd-2020-304, https://gmd.copernicus.org/preprints/gmd-2020-304/, 2020.

Mastin, L., Guffanti, M., Servranckx, R., Webley, P., Barsotti, S., Dean, K., Durant, A., Ewert, J., Neri, A., Rose, W., Schneider, D., Siebert, L., Stunder, B., Swanson, G., Tupper, A., Volentik, A., and Waythomas, C.: A multidisciplinary effort to assign realistic source parameters to models of volcanic ash-cloud transport and dispersion during eruptions, Journal of Volcanology and Geothermal Research, 186, 10 – 21, https://doi.org/https://doi.org/10.1016/j.jvolgeores.2009.01.008, http://www.sciencedirect.com/science/article/pii/S0377027309000146, improved Prediction and Tracking of Volcanic Ash Clouds, 2009.

Maters, E. C., Delmelle, P., and Bonneville, S.: Atmospheric Processing of Volcanic Glass: Effects on Iron Solubility and Redox Speciation, Environmental Science & Technology, 50, 5033–5040, https://doi.org/10.1021/acs.est.5b06281, 2016.

Maters, E. C., Delmelle, P., and Gunnlaugsson, H. P.: Controls on iron mobilisation from volcanic ash at low pH: Insights from dissolution experiments and Mössbauer spectroscopy, Chemical Geology, 449, 73 – 81, https://doi.org/https://doi.org/10.1016/j.chemgeo.2016.11.036, http://www.sciencedirect.com/science/article/pii/S0009254116306465, 2017.

Menut, L., Bessagnet, B., Khvorostyanov, D., Beekmann, M., Blond, N., Colette, a., Coll, I., Curci, G., Foret, G., Hodzic, a., Mailler, S., Meleux, F., Monge, J.-L., Pison, I., Siour, G., Turquety, S., Valari, M., Vautard, R., and Vivanco, M. G.: CHIMERE 2013: a model for regional atmospheric composition modelling, Geoscientific Model Development, 6, 981–1028, https://doi.org/10.5194/gmd-6-981-2013, http://www.geosci-model-dev.net/6/981/2013/, 2013.

Menut, L., Bessagnet, B., Briant, R., Cholakian, A., Couvidat, F., Mailler, S., Pennel, R., Siour, G., Tuccella, P., Turquety, S., and Valari, M.: The CHIMERE v2020r1 online chemistry-transport model, Geoscientific Model Development Discussions, 2021, 1–50, https://doi.org/10.5194/gmd-2021-96, https://gmd.copernicus.org/preprints/gmd-2021-96/, 2021.

NCEP: NCEP GFS 0.25 Degree Global Forecast Grids Historical Archive, https://doi.org/10.5065/D65D8PWK, 2015.

Pattantyus, A. K., Businger, S., and Howell, S. G.: Review of sulfur dioxide to sulfate aerosol chemistry at Kilauea Volcano, Hawaii, Atmospheric Environment, 185, 262–271, https://doi.org/https://doi.org/10.1016/j.atmosenv.2018.04.055, 2018.

Pianezze, J., Tulet, P., Foucart, B., Leriche, M., Liuzzo, M., Salerno, G., Colomb, A., Freney, E., and Sellegri, K.: Volcanic Plume Aging During Passive Degassing and Low Eruptive Events of Etna and Stromboli Volcanoes, Journal of Geophysical Research: Atmospheres, 124, https://doi.org/10.1029/2019JD031122, https://agupubs.onlinelibrary.wiley.com/doi/abs/10.1029/2019JD031122, 2019.

Pollack, J. B., Toon, O. B., Danielsen, E. F., Hofmann, D. J., and Rosen, J. M.: The El Chichon volcanic cloud: An introduction, Geophysical Research Letters, 10, 989–992, https://doi.org/10.1029/GL010i011p00989, 1983.

Roberts, T., Dayma, G., and Oppenheimer, C.: Reaction Rates Control High-Temperature Chemistry of Volcanic Gases in Air, Frontiers in Earth Science, 7, 154, https://doi.org/10.3389/feart.2019.00154, https://www.frontiersin.org/article/10.3389/feart.2019.00154, 2019.

Sahyoun, M., Freney, E., Brito, J., Duplissy, J., Gouhier, M., Colomb, A., Dupuy, R., Bourianne, T., Nowak, J. B., Yan, C., Petäjä, T., Kulmala, M., Schwarzenboeck, A., Planche, C., and Sellegri, K.: Evidence of New Particle Formation Within Etna and Stromboli Volcanic Plumes and Its Parameterization From Airborne In Situ Measurements, Journal of Geophysical Research: Atmospheres, 124, 5650–5668, https://doi.org/https://doi.org/10.1029/2018JD028882, https://agupubs.onlinelibrary.wiley.com/doi/abs/10.1029/2018JD028882, 2019.

Salerno, G., Burton, M., Oppenheimer, C., Caltabiano, T., Randazzo, D., Bruno, N., and Longo, V.: Three-years of SO2 flux measurements of Mt. Etna using an automated UV scanner array: Comparison with conventional traverses and uncertainties in flux retrieval, Journal of Volcanology and Geothermal Research, 183, 76 – 83, https://doi.org/https://doi.org/10.1016/j.jvolgeores.2009.02.013, http://www.sciencedirect.com/science/article/pii/S0377027309000791, 2009.

Salerno, G. G., Burton, M., Di Grazia, G., Caltabiano, T., and Oppenheimer, C.: Coupling Between Magmatic Degassing and Volcanic Tremor in Basaltic Volcanism, Frontiers in Earth Science, 6, 157, https://doi.org/10.3389/feart.2018.00157, https://www.frontiersin.org/article/10.3389/feart.2018.00157, 2018.

Sander, R.: Compilation of Henry's law constants (version 4.0) for water as solvent, Atmospheric Chemistry and Physics, 15, 4399–4981, https://doi.org/10.5194/acp-15-4399-2015, https://acp.copernicus.org/articles/15/4399/2015/, 2015.

Seinfeld, J. H. and Pandis, S. N.: ATMOSPHERIC From Air Pollution to Climate Change SECOND EDITION, Wiley-interscience publication, 2006.

Sellitto, P., Zanetel, C., di Sarra, A., Salerno, G., Tapparo, A., Meloni, D., Pace, G., Caltabiano, T., Briole, P., and Legras, B.: The impact of Mount Etna sulfur emissions on the atmospheric composition and aerosol properties in the central Mediterranean: A statistical analysis over the period 2000–2013 based on observations and Lagrangian modelling, Atmospheric Environment, 148, 77 – 88, https://doi.org/https://doi.org/10.1016/j.atmosenv.2016.10.032, http://www.sciencedirect.com/science/article/pii/S1352231016308391, 2017.

Sellitto, P., Salerno, G., La Spina, A., Caltabiano, T., Scollo, S., Boselli, A., Leto, G., Zanmar Sanchez, R., Crumeyrolle, S., Hanoune, B., and Briole, P.: Small-scale volcanic aerosols variability, processes and direct radiative impact at Mount Etna during the EPL-RADIO campaigns, Scientific Reports, 10, https://doi.org/10.1038/s41598-020-71635-1, https://doi.org/10.1038/s41598-020-71635-1, 2191.

Shinohara, H., Aiuppa, A., Giudice, G., Gurrieri, S., and Liuzzo, M.: Variation of H2O/CO2 and CO2/SO2 ratios of volcanic gases discharged by continuous degassing of Mount Etna volcano, Italy, Journal of Geophysical Research: Solid Earth, 113, https://doi.org/10.1029/2007JB005185, https://agupubs.onlinelibrary.wiley.com/doi/abs/10.1029/2007JB005185, 2008.

Shostak, S., Kim, K., Horbatenko, Y., and Choi, C. H.: Sulfuric Acid Formation via H2SO3 Oxidation by H2O2 in the Atmosphere, The Journal of Physical Chemistry A, 123, 8385–8390, https://doi.org/10.1021/acs.jpca.9b05444, https://doi.org/10.1021/acs.jpca.9b05444, pMID: 31486645, 2019.

Skamarock, W. C., Klemp, J. B., Dudhia, J., Gill, D. O., Barker, D. M., Duda, M. G., Huang, X.-Y., Wang, W., and Powers, J. G.: A Description of the Advanced Research WRF Version 3., Tech. rep., NCAR, https://doi.org/doi:10.5065/D68S4MVH, 2008.

Textor, C., Graf, H.-F., Herzog, M., and Oberhuber, J. M.: Injection of gases into the stratosphere by explosive volcanic eruptions, Journal of Geophysical Research: Atmospheres, 108, https://doi.org/10.1029/2002JD002987, https://agupubs.onlinelibrary.wiley.com/doi/abs/10.1029/2002JD002987, 2003.

Van Leer, B.: Towards the ultimate conservative difference scheme. IV. A new approach to numerical convection, Journal of Computational Physics, 23, 276 – 299, https://doi.org/https://doi.org/10.1016/0021-9991(77)90095-X, http://www.sciencedirect.com/science/article/pii/002199917790095X, 1977.